UNIVERSITY OF CALIFORNIA

Santa Barbara

Study of the Capture and Release of Uranyl or Lanthanide using Redox-Active Carboranes

A Thesis submitted in partial satisfaction of the

requirements for the degree Master of Science

in Chemistry

by

Chae Yeong Kim

Committee in charge:

Professor Gabriel Ménard, Chair

Professor Trevor Hayton

Professor Mahdi Abu-Omar

December 2022

_____

Professor Trevor W. Hayton

_____

Professor Mahdi Abu-Omar

_____

Professor Gabriel Ménard, Committee Chair

December 2022

Study of the Capture and Release of Uranyl or Lanthanide using Redox-Active Carboranes

by

Chae Yeong Kim

ACKNOWLEDGEMENTS

I would like to thank Dr. Gabriel Menard for guiding me as a teacher, a mentor and a personal instructor with great patience. You set up a whole new standard as a PI and I learned so much of knowledge as well as the attitude as a graduate student.

Thank you to the Gab Lab members who have helped with my thesis and giving me ideas for experiments.

Special thanks to Korean friends who helped me a lot to settle down to a new environment, giving me shelter, food and a lot of memory to remember.

Thank you to my other friends and former roommates who had given me good time.

Thank you to all staff and faculty of chemistry department, who helped me deal with my decision about Ph.D. program. I thank Guang who helped me a lot for getting those crystal structures.

Thank you for my family who have been backing me up when I need it.

ABSTRACT

Study of the Capture and Release of Lanthanide or Uranyl using Redox-Active Carboranes

by

Chae Yeong Kim

For the first part of this work, we explored the potential of repetitively cycling the *ortho*-substituted carborane, 1,2-(Ph2PO)$_2$-1,2-$C_2B_{10}H_{10}$ (**^{PO}Cb**), by galvanostatic bulk electrolysis (GBE) to capture and release the uranyl cation, UO_2^{2+}. The metal capturing process worked successfully for the first cycle of GBE and captured UO_2^{2+} successfully in the form of $[UO_2(^{PO}Cb)_2]$. However, the second cycle of the GBE using the same ^{PO}Cb, does not show a significant amount of reduced ^{PO}Cb. The results show different side-products form after the second reduction step indicating that the second charge cycle to generate *nido*-**^{PO}Cb,** the reduced form of **^{PO}Cb** was unsuccessful. By treating with different methods of extraction during the cycle of GBE, we were able to gain some understanding about what is hindering the second reduction. From series of experiments, we determined that a water adduct forms with *closo*-^{PO}Cb and this hinders the ability of *closo*-^{PO}Cb to be reduced properly, and therefore we could not capture much uranyl in the second cycle. These results are presented herein.

The second part of the thesis investigates the capture of different lanthanide metals using *nido*-$^{PO}Cb^{2-}$. Surprisingly, each lanthanide with *nido*-^{PO}Cb shows different coordination even though we added the same equivalents, 2.1:1. X-ray diffraction studies confirmed the different

coordination environments. While the nature of this coordination remains under investigation, we suspect that the high reduction potential of the lanthanide metal is likely at play. Further experiments were conducted to back up the idea.

TABLE OF CONTENTS

LIST OF FIGURES

LIST OF SCHEMES

LIST OF TABLES

Chapter 1

Introduction

1.1 Carboranes

1.1.1 *Ortho*-carborane

Carboranes are polyhedral boron-carbon clusters that have applications in many fields such as metal-ion extraction, catalysis, luminescence, optoelectronic applications, and energy storage applications.[1] There are different types of cage-like carboranes such as $C_2B_3H_5$, $C_2B_3H_5$, $C_2B_5H_7$, and CB_5H_7.[2] Among the diverse types of carboranes, *ortho*-carborane (*o*-carborane, $C_2B_{10}H_{12}$ = Cb, **Figure 1.1**), reported in 1963[3] possesses desirable properties such as thermal and redox stability, chemical inertness, and low nucleophilicity.[4]

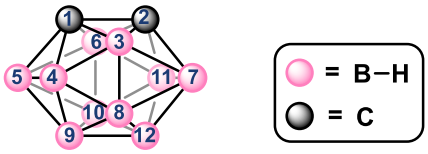

1,2 $C_2B_{10}H_{12}$

Figure 1.1. *Ortho*-carborane.

Its stability is gained by electron-delocalized covalent bonds. Among the localized electron-pair bonds, electrons in carboranes are delocalized among the skeletal boron and carbon atoms. Therefore, the carbon and boron atoms in carborane can have bonding that is non-classical. For example, carbon and boron in carborane can have at least 3 and as many as 6 neighboring atoms. In the case of *o*-carborane, one atom has 5 neighboring atoms.

1.1.2 *Closo-ortho*-carborane and *nido-ortho*-carborane

The prefix *closo*- in *closo*-carborane refers to the carborane cage that has a closed polyhedron geometry with all faces equatorial triangles. For *closo*-carborane, the skeletal

electron pairs (SEP) that make up the cluster's delocalized -bonding framework is based on the number of vertices (n) under the equation SEP = n + 1. *Nido*-carborane refers to an n + 2 polyhedral carborane cage with 1 missing vertex.

In this chapter, we will be talking about *ortho*-carboranes which indicate carboranes containing 12 vertexes, and 2 carbons placed at positions 1, 2**. (Figure 1.1)**. Its charge is neutral and with SEP being 13, has a skeletal electron number of 26. On the other hand, *nido*-carborane contains a 12 vertex caged carborane that has gone through complete cleavage of the cage C–C bond from the *closo*-Cb. Therefore, it is missing one vertex compared to *closo*-Cb having 13 vertices and has 2 more electrons than *closo*-, resulting in a -2 total charge **(Figure 1.2)**.[5]

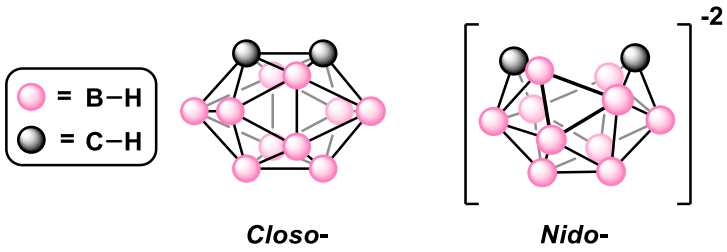

Figure 1.2. (left) *closo-ortho*-carborane (*closo*-Cb). (right) *nido-ortho*-carborane (*nido*-Cb)

1.1.3 *Ortho*-carborane Redox

Studies have shown that the neutral *closo*-Cb can undergo $2e^-$ reduction, increasing the SEP to 14, and the total number of skeletal electrons to 28, therefore, resulting in a change in the cluster geometry.[4,6] During this process, the C–C bond in *closo*-Cb breaks, leading to the cage opening to form the open *nido*-Cb ($C_2B_{10}H_{12}^{2-}$) which still has 12 vertices but with 2 extra cluster electrons. The *nido*-Cb can be oxidized back to *closo*-Cb, recovering C-C bond again, showing its redox switchable property.[1]

At the carbon part of the *closo*-Cb, it can be readily substituted with different functional groups due to the acidity of the C-H which is attributed to the inductive effect caused by the electron-deficient framework. In this sense, donor ligands for capturing metals may be attached to each carbon atom of the carborane. After the reduction of *closo*-Cb, the ligand bite angle significantly increases compared to its neutral *closo*-form (**Figure 1.3**). The bigger bite angle in *nido*-Cb enables better metal coordination, while the *closo*-form may have poor metal binding ability due to the smaller bite angle. We previously reported the use of such redox-switchable coordinating abilities for the electrochemical capture and release of uranyl (M = UO_2^{2+}) from biphasic solutions (**Figure 1**).[1] By utilizing this biphasic redox-switching function from the *closo*- to the *nido*-Cb, we may suggest a new method to capture and release metals from spent nuclear fuel.[1,7,8]

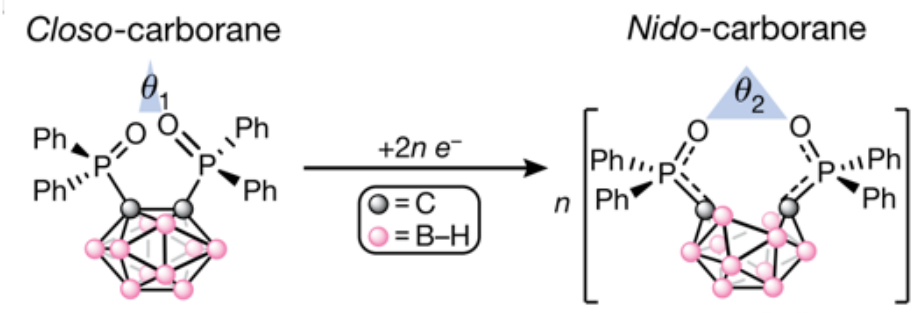

Figure 1.3 Changes in relative bite angles (θ) between *closo*-Cb and *nido*-Cb

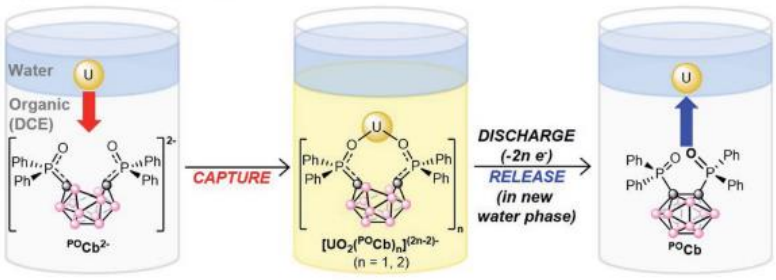

Figure 1.4 Capture and release of metal cation using Cb with Galvanostatic bulk electrolysis

1.1.4 Electronic study of substituted Cb

The reduction of Cb is a key property for the applicability of Cb-based chemistry for repeatable metal capture/release (**Figure 1**), highlighting the importance to study the electronic properties of the substituted Cb. *o*-Cb has a reported reduction potential at -2.96 V vs. Fc/Fc^+ (Fc = ferrocene).[9] The comparatively low reduction potential suggests less stability of *nido*-Cb, especially under aqueous conditions. The reduction potential of *ortho*-Cb can be shifted by changing the electronic nature of the substituents on boron or carbon by adding functional groups to it. [4] For example, Cb with a chloride substitution on the 9-position (9-Cl-Cb) has a more positive reduction potential at -2.34 V vs SCE.[9] The second chlorine substitution on the 12-position (9, 12-Cl_2-Cb) shifted the reduction potential anodically to -2.03 V (오류! 참조 원본을 찾을 수 없습니다.). Overall, modifying the electronic nature of the substituents enables control of the redox potentials for the reduction of diverse substituted Cb. As diphenyl phosphine oxide ligand has been substituted on carbon, the redox potential becomes much more positive (-0.994 V vs. Fc/Fc^+),[1] indicating that it is much easier reduce and the reduced form is much stable. For this reason, diphenylphosphine oxide substituted Cb has been used in all the experiments in this thesis.

The structural change caused by the C–C bond cleavage during reduction affects the electrochemical and chemical redox reversibility of the Cb, which is further dependent on the nature of the substituents.[4] The 2 e^- reduction of substituted Cb can occur simultaneously or in two steps, depending on the stability of the mono-reduced radical intermediate.

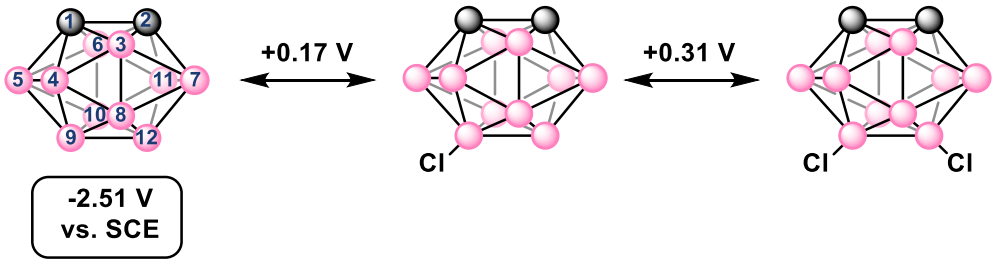

Figure 1.1. Chloride substitution on the Cb cage shifts the reduction potential

1.2 Uranyl Capture

1.2.1 Uranium Metal

Nuclear energy is utilized as a large and important part of the world's energy. It is contributing 11% of all electricity worldwide.[10] While nuclear energy is often considered a low-carbon energy alternative to fossil fuels,[11] the disposal of spent nuclear fuel (SNF) makes this technology imperfect. Uranium is normally in its dioxide form (UO_2) in nuclear fuel, and composes 95% of the waste in SNF. The remaining waste is from the fission products generated including Pu (0.9%); the minor actinides (0.1% (Np, Am, Cm)); lanthanides, Tc, Mo, I, Cs, and others (together ca. 4%).[12] Approximately huge amount of SNF (450,000 tons) have been generated worldwide so far and only 25% have been reprocessed using the Plutonium Uranium Redox Extraction (PUREX) process which has been used for decades.

1.2.2 PUREX Process

The PUREX Process is a commercially used liquid-liquid extraction process that is quite efficient at extracting and recycling UO_2^{2+} to reduce SNF waste. The downside of PUREX involves additional selective extraction of a pure Pu stream and the waste from the process is highly radiotoxic, which raises significant proliferation concerns from major stakeholders, such as the U.S.[14] While other reprocessing schemes addressing these concerns have been

developed such as UREX[12], none of them are commercial so far. To this day, the proliferation concerns has taken the place of reprocessing efforts in places like the U.S., forcing countries to instead increase their SNF storage capacity, and thus putting back action on the nuclear waste issue. [15]

1.3 Lanthanides

1.3.1. Lanthanide metals

Rare Earth Elements (REE) are the 15 elements that make up the f orbital filling portion of row 6 of the periodic table. That group of elements is also commonly referred to as lanthanides. Lanthanides have been utilized in many applications such as batteries, permanent magnets for hybrid vehicles and wind turbines, fluid cracking catalysts for gas production and imaging, and therapeutic agents for cancer diagnosis and treatment. [16] Lanthanides contain f-orbital electrons giving rise to their exceptional magnetic properties, and therefore substitutions outside the REE (Rare Earth Elements) family for these applications are often difficult to impossible. [18]

China has been a key supplier and consumer of lanthanides, and with an increasing demand for lanthanides in electronics, some worry that diminishing supply could cause hindrance to modern technology development. To address this, there is new interest in developing technology that would mitigate the shortage of lanthanide metals.[17] Despite their diverse magnetic and electronic properties, Ln^{3+} ions (Ln = Lanthanide) have a strong preference for the +3 oxidation state, and the tendency to engage in ionic bonding explains the similar chemical properties among lanthanides.[18,19] The major distinguishing feature among them is their ionic radius, which decreases across the series (size decreases from left to right), a phenomenon known as the lanthanide contraction.[20]

1.3.2 Lanthanide capture

Chelators are commonly used to capture 4f metal ions (Lanthanide). Ethylene diamine tetra-acetic acid (EDTA) and its derivatives 1,4,7,10-tetraazacyclododecane-1,4,7,10-tetraacetic acid (DOTA) and diethylene tri-amine penta-acetic acid (DTPA) exhibit high affinity for lanthanide metals and these chelators have been used for decades for their superior luminescence intensities, and more recently, for NMR experiments (**Figure 1.6**).[21,22,23] They are known to form 1:1 complexes that exhibit high thermodynamic stability and kinetic inertness.

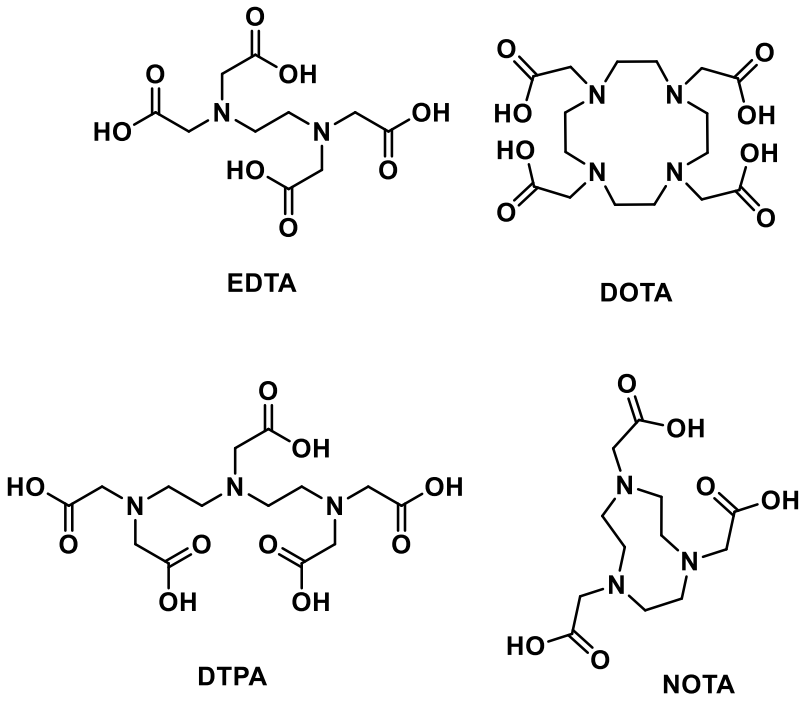

Figure 1.6 Chelators for lanthanide metal

DOTA is one of the primary working chelators for radiometal chemistry and is one of the current ‘‘gold standards’’ for chelating a number of isotopes, including Lu.[17] However, DOTA

has been widely accepted to be less stable than its more petite macrocyclic counterpart NOTA. (axially symmetric macrocyclic triaza ligand 1,4,7-triazacyclononiane-N, N′, N″-triacetic acid). [24] In the case of DOTA and NOTA, complex coordination is maintained via free electron pairs of hetero elements as well as via carboxylate groups and is mainly influenced by pH, temperature, and concentration.[25] DOTAGA (GA= glutaric acid)[26] and various isothiocyanate derivatives of DOTA have been also synthesized. These DOTA derivatives retain their maximum potential denticity (octadentate) as well as the same thermodynamic stability and kinetic inertness. **(Figure 1.6)**.

The coordination chemistry and properties of Ln^{3+} preferentially form 8–9 coordinate complexes in square anti- prismatic or monocapped square antiprismatic geometries. They are considered hard metal cations with a preference for hard ligand donors such as carboxylate-oxygens and amine-nitrogens. A historical glance at previous work reveals that macrocycles are generally more kinetically inert than acyclic chelators, even if their thermodynamic stabilities have been determined to be very similar. This has to be considered when designing new chelators. Macrocyclic chelators require minimal reorganization energy during metal ion coordination, as they show inherently constrained geometries and partially pre-organized metal ion binding sites, thereby go through decreasing the entropic loss upon metal ion coordination. In contrast, acyclic chelators must undergo more drastic changes in physical orientation and geometry for donor atoms to coordinate with the metal ion. Eventually they suffer a more significant decrease in entropy than do macrocycles (thermodynamically unfavorable). Therefore, the thermodynamic driving force towards complex formation is greater for macrocycles in general, a phenomenon referred to as the macrocycle effect.[27] However, acyclic

chelators outstands at coordination kinetics and radiolabeling efficiency whereas macrocycles tend to suffer.[28]

1.4 Scope of thesis

In this thesis, we have explored the potential for repeated metal capture of uranyl featuring diphenyl phosphine oxide *ortho*-carborane. We first sought to find whether the diphenylphosphineoxide (^{PO}Cb) can be reused again by studying more than one cycle of galvanostatic bulk electrolysis (GBE) for capture. We suspect that the side products that have been produced during the first GBE cycle are hindering the ^{PO}Cb to be reduced again during subsequent GBE cycles. ^{31}P NMR experiments were conducted to track the reusability of ^{PO}Cb and side products (Chapter 2).

We further extended our study on coordination environments on the lanthanide metals with diphenyl phosphine oxide substituted Cb. We have discovered that the coordination environments are different depending on lanthanide metals and this is a surprising result considering lanthanide metals are known for similar chemical behavior. Further investigation of the study may open up new avenues for RE(Rare Earth) separations by investigating a new redox-switchable system to capture and release lanthanide metals (Chapter 3).

In Chapters 2-3, all compounds were prepared and characterized by the author. All NMR experiments and GBE experiments were performed by the author. The electrochemical methods were adapted from Mattejat and Keener et. al [1,7]and performed by the author.

1.5 References

(1) Keener, M.; Hunt, C.; Carroll, T. G.; Kampel, V.; Dobrovetsky, R.; Hayton, T. W.; Ménard, G. Redox-Switchable Carboranes for Uranium Capture and Release. *Nature* **2020**, *577* (7792), 652–655.

(2) Williams, R. E. Carborane Polymers. *Pure Appl. Chem.* **1972**, *29* (4), 569–584.

(3) Fein, B. M. M.; Grafstein, D.; Faustian, J. E.; Bobinski, J.; Lichstein, B. M.; Mayes, N.; Schwartz, N. N. 1,2-Substituted. **1963**, *2* (6).

(4) Núñez, R.; Tarrés, M.; Ferrer-Ugalde, A.; De Biani, F. F.; Teixidor, F. Electrochemistry and Photoluminescence of Icosahedral Carboranes, Boranes, Metallacarboranes, and Their Derivatives. *Chem. Rev.* **2016**, *116* (23), 14307–14378.

(5) Roca-Sabio, A.; Mato-Iglesias, M.; Esteban-Gómez, D.; Toth, É.; De Bias, A.; Platas-Iglesias, C.; Rodríguez-Blas, T. Macrocyclic Receptor Exhibiting Unprecedented Selectivity for Light Lanthanides. *J. Am. Chem. Soc.* **2009**, *131* (9), 3331–3341.

(6) Fisher, S. P.; Tomich, A. W.; Lovera, S. O.; Kleinsasser, J. F.; Guo, J.; Asay, M. J.; Nelson, H. M.; Lavallo, V. Nonclassical Applications of Closo-Carborane Anions: From Main Group Chemistry and Catalysis to Energy Storage. *Chem. Rev.* **2019**, *119* (14), 8262–8290.

(7) Keener, M.; Mattejat, M.; Zheng, S. L.; Wu, G.; Hayton, T. W.; Ménard, G. Selective Electrochemical Capture and Release of Uranyl from Aqueous Alkali, Lanthanide, and Actinide Mixtures Using Redox-Switchable Carboranes. *Chem. Sci.* **2022**, *13* (12), 3369–3374.

(8) Bruno, J.; Ewing, R. C. Spent Nuclear Fuel. *Elements* **2006**, *2* (6), 343–349.

(9) Morris, J. H.; Gysling, H. J. Electrochemistry of Boron Compounds Ph3B Ph : B--- Ph3B2--. **1985**, 51–76.

(10) International Atomic Energy Agency (IAEA). Nuclear Power and the Paris Agreement. *Iaea* **2016**, 10.

(11) Adamantiades, A.; Kessides, I. Nuclear Power for Sustainable Development: Current Status and Future Prospects. *Energy Policy* **2009**, *37* (12), 5149–5166.

(12) Kumari, I.; Kumar, B. V. R.; Khanna, A. A Review on UREX Processes for Nuclear Spent Fuel Reprocessing. *Nucl. Eng. Des.* **2020**, *358* (June 2019), 110410.

(13) Paviet-hartmann, P. Catherine R., Keri C., Edward M. Overview of Reductants Utilized in Nuclear Fuel Reprocessing / Recycling Global **2013**

(14) Lanham, W. B.; Runion, T. C. PUREX Process for Plutonium and Uranium Recovery. *Oak Ridge Natl. Lab.* **1949**, *479* (October), 1–12.

(15) Konings, R. J. M.; Stoller, R. E. Comprehensive Nuclear Materials. *Compr. Nucl. Mater. Second Ed.* **2020**, 1–4653.

(16) Thiele, N. A.; Fiszbein, D. J.; Woods, J. J.; Wilson, J. J. Tuning the Separation of Light Lanthanides Using a Reverse-Size Selective Aqueous Complexant. *Inorg. Chem.* **2020**, *59* (22), 16522–16530.

(17) Nassar, N. T.; Du, X.; Graedel, T. E. Criticality of the Rare Earth Elements. *J. Ind. Ecol.* **2015**, *19* (6), 1044–1054.

(18) Cotton, S. A. Scandium, Yttrium & the Lanthanides: Inorganic & Coordination Chemistry; Uppingham School, **2011**

(19) Huang, C.; Earth, R.; Chemistry, C. *Rare Earth Coordination*; John Wiley & Sons (Asia) Pte Ltd. , **2010.**

(20) Seitz, M.; Oliver, A. G.; Raymond, K. N. The Lanthanide Contraction Revisited of Incomplete Series Including Solid-State Materials, 4 as Well As. *J. Am. Chem. Soc.* **2007**, *129* (36), 11153–11160.

(21) Fusaro, L.; Mocci, F.; Muller, R. N.; Luhmer, M. Insight into the Dynamics of Lanthanide-DTPA Complexes As Revealed by Oxygen-17 NMR. *Inorg. Chem.* **2012**. *51*, 8455−8461

(22) William, B.; Horrocks, D. E. W. Luminescence Spectroscopy *METHODS IN ENZYMOLOGY*, **1993** *226* p495

(23) Brittain, G.; Richardson, S.; Bruce, R.; Burtnick, D. Circularly Polarized Emission Of Terbium(Ii1) Substituted-C, *Biochemical And Biophysical Research Communications* **1976**, *68* (3), 1013–1019.

(24) Geraldes, C. F. G. C.; Singh, M.; Sherry, A. D. Lanthanide-Nota Chelates As Aqueous Shift Reagents: Interaction With Cyclopropane Carboxylic Acid* *Journal of the Less-Common Metals*, **1985**, *112*, 255–261.

(25) Kretschy, D.; Koellensperger, G.; Hann, S. Stability Assessment of Different Chelating Moieties Used for Elemental Labeling of Bio-Molecules. *Metallomics* **2011**, *3*, 1304–1309.

(26) Bernhard, C.; Moreau, M.; Lhenry, D.; Goze, C.; Boschetti, F.; Rousselin, Y.; Brunotte, F.; Denat, F. DOTAGA – Anhydride : A Valuable Building Block for the Preparation of DOTA-Like Chelating Agents. *Chem. Eur. J.* **2012**, *18*, 7834 – 7841

(27) Shriver, D., Weller, M., Overton, T., Rourke J., Armstrong F. Inorganic Chemistry 6th edition **2014**

(28) Hu, A.; Macmillan, S. N.; Wilson, J. J. Macrocyclic Ligands with an Unprecedented Size-Selectivity Pattern for the Lanthanide Ions. *J. Am. Chem. Soc.* **2020,** *142*, 13500−13506.

(29) Nguyen-trung, C.; Humbert, B. Hydrolysis of Uranyl (VI) in Acidic and Basic Aqueous Solutions Using a Noncomplexing Organic Base : A Multivariate Spectroscopic and Statistical Study. *Inorg. Chem.* **2011**, *No.6*, 2811–2823.

(30) Pant, D. D., Handelwal D. P. The absorption and fluorescence spectra of uranyl nitrate solutions at room temperature., D.S.B. Government College, **1959**, 323–335.

(31) Hunt, C.; Mattejat, M.; Anderson, C.; Sepunaru, L.; Me, G. Symmetric Phthalocyanine Charge Carrier for Dual Redox Flow Battery/Capacitor Applicationś. *ACS Appl. Energy Mater.* **2019,** 5391-5396

Chapter 2

Exploring continuous cycling of galvanostatic bulk electrolysis of diphenylphosphine oxide substituted *o*-carborane

2.1 Introduction

Previously we have shown that reduction of *closo*-Cb to the *nido*-Cb results in cleavage of the C-C bond and an increasing the bite angle between the substituted donor ligand. The increased bite angle enables the capture of different metals.[1] Diphenyl phosphine oxide substituted *o*-carborane was applied to the biphasic electrochemical selective capture and release of UO_2^{2+} from spent nuclear fuel mimics.[2] UO_2^{2+} was captured in the *nido*-form and released in the *closo*-form. The Cb-based capture was done in monophasic condition initially and then further extended and has been achieved in biphasic condition by extracting UO_2^{2+} from aqueous solution to organic DCE solution containing the *nido*-Cb that was generated electrochemically. After removal of the aqueous layer post capturing UO_2^{2+}, the organic layer underwent electrochemical oxidation to regenerate *closo*-Cb and a freshwater layer was added to extract the released UO_2^{2+}. Cb-based capture/release cycling was selective towards UO_2^{2+} over other heavy metal ions from the aqueous layer that mimic spent nuclear fuel which contained Cs^+, Nd^{3+}, Sm^{3+}, Th^{4+}, UO_2^{2+}.[2] The selective coordination of *nido*-Cb with UO_2^{2+} was determined by ^{31}P NMR and ICP-OES studies. However, during the electrochemical cycling, loss of *closo*- and *nido*- Cb was observed in each cycle step. At the same time, we detected an unknown side product in the ^{31}P NMR spectrum at 45 ppm and a 0.5 ppm chemical shift of *closo*-Cb after exposing the carboranes to the aqueous solution. Previously, they have not yet explored whether the biphasic GBE is possible repeatedly with the same solution of ^{PO}Cb and continuously capture UO_2^{2+} if we continue to supply it. Recyclability is very important from the perspective of economic and environmental issues. In this chapter, we have

discovered that reusing the same ^{PO}Cb is not successful and tried to answer what is causing the diminishing amount of *clos*o and *nido* Cb.

2.2 Results and Discussion

2.2.1 Synthesis of 1,2-$(Ph_2PO)_2$-1,2-$C_2B_{10}H_{10}$, ^{PO}Cb (1)

We first synthesized 1,2-$(Ph_2PO)_2$-1,2-$C_2B_{10}H_{10}$ (^{PO}Cb (**1**)) according to our previous procedure.[1] We started with commercially available *ortho*-carborane and deprotonating with *n*-butyllithium followed by treatment to diphenylphosphine chloride in diethyl ether solvent. The product was purified by column chromatography and then the phosphorous on carbon was oxidized with oxidant H_2O_2 to give the final product, **1** (**Scheme 2.1**). It was recrystallized with hot acetonitrile. The final product was confirmed with ^{1}H, ^{31}P{^{1}H}, ^{11}B NMR spectroscopy and matched literature values.[1,2]

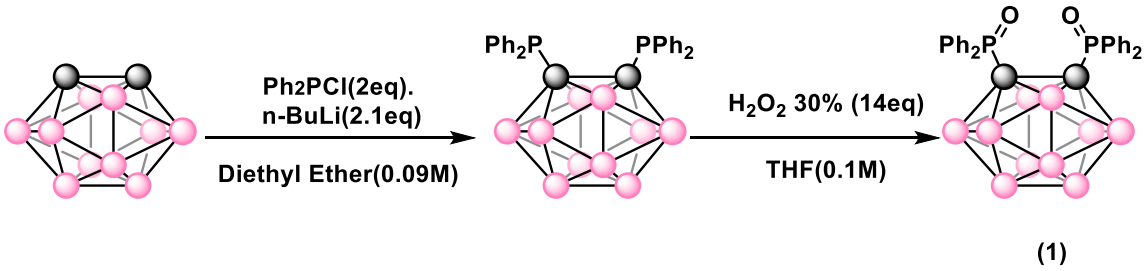

Scheme2.1 Synthesis of ^{PO}Cb **(1)**

2.2.2. Method (I): Electrolysis with UO_2^{2+} in NaOAc buffer solution (pH = 5.4)

To answer whether repeated GBE cycling of **1** is possible or not, we had to test if a used **1** solution could be reduced a second time after going through one cycle of GBE. The procedure for GBE cycle experiment followed our previous GBE experiments done by our group.[1,2] The synthesized **1** was used in the electrolysis with UO_2^{2+} in NaOAc buffer solution (pH=5.4). The

NaOAc buffer solution was used to mimic our previous experiments done by our group which required the use of a buffer to control for the pH-dependent extinction coefficient (ϵ) of UO_2^{2+} which was monitored by UV- vis spectroscopy[3,4] and to compare the extraction efficacy of our system at varying pH values. 1,2-dichloroethane (DCE) solutions were next loaded with **1** (1 equiv.), [PPN][PF_6] (0.5 equiv. $[PPN]^+$ = $[Ph_3PNPPh_3]^+$) as internal standard for NMR spectroscopy and [Bu_4N][PF_6] (0.1 M) as supporting electrolyte, and were loaded into one of two compartments of divided H- cells. Each counter compartment was loaded with a heterogeneous carbon additive (Ketjenblack) which served as a capacitive buffer[28] and which was mixed in DCE with 0.1 M [Bu_4N][PF_6]. All H-cells were configured with physical glass-frit separators and contained carbon electrodes on each side. The solutions of **1** were electrochemically reduced by GBE to a theoretical state-of-charge (SOC) of *ca.* 75% assuming a 100% coulombic efficiency. Subsequent analyses of the carborane solutions by unlocked $^{31}P\{^1H\}$ NMR spectroscopy revealed the clean conversion of **1** to the reduced $^{PO}Cb^{2-}$ in approximate *ca.*70 % yield which is in line with the SOC.

In this work, we have gone through one more step from previous GBE cycle that a second GBE charge was applied. However, the result were not promising to repeatedly run GBE to capture UO_2^{2+} since there was only little amount of *nido*-^{PO}Cb left after the second charge (8.0 %) compared to the starting amount of **1**. Seeing this result, we have extracted with different extraction methods to compare the different results and side products forming so we could understand what is hampering the second reduction of the GBE cycle. The different extraction methods applied are: each charged solution is removed from its respective H-cell and mixed with either: I) a NaOAc-buffered (pH = 5.4) aqueous solution with 1.25 equiv. of

UO_2^{2+}relative to **1**; II) a NaOAc-buffered (pH = 5.4) aqueous with no UO_2^{2+}in thesolution; III) with the aqueous solution with no buffer, or; IV) lastly control experiment that does not get in contact with any aqueous buffer solution nor UO_2^2.

Throughout the GBE process of all the methods **(I, II, III, IV)**, significant yellowing of the organic phases was observed after the first GBE charge. All experiments were analyzed by unlocked ^{31}P NMR spectroscopy of the organic DCE layer. With all different methods applied, all the unlocked ^{31}P NMR spectra below (**Figure 2.1**) are monitored in the order of the GBE process like this: (A) before mixing with the organic phases; (B) after charging; (C) following with buffer solution mixing; (D) after discharge; (E) mixing with buffer solution after discharge; (F) after the second charge with the GBE electrolysis.

The synthesized *closo*-^{PO}Cb was used in electrolysis with UO_2^{2+} in NaOAc buffer solution (pH = 5.4) of the GBE cycle. All the peaks shown from steps (A) to (E) are the same as compared in our previous study.[2] All the percentages of Cb amount calculated are based on starting material, *closo*-^{PO}Cb amount in ^{31}P{^{1}H} NMR of step (A) and calculated assuming that PPN does not degrade or lost during GBE or extraction process. In step (B), *nido*-^{PO}Cb formed and some residue *closo*- ^{PO}Cb peak is shown. In step (C), after charging and stirred with UO_2^{2+} solution, it showed some peaks at 52.0 ppm indicating the formation of $[UO_2(POCb)_2]^{2-}$, as well as some minor peaks $[Bu_4N][^{PO}CbH]$ (denoted as *(red), 25.7 ppm, 28.5 ppm)[2] and showing unknown side product at 45.3 ppm (green star, *) It is notable that after exposing the organic layer to buffer solution containing metal, the peak of *closo*- ^{PO}Cb in ^{31}P NMR is shifted to left about 0.5 ppm and remained shifted for the rest of the steps. In step (D), a broad peak for *closo*- ^{PO}Cb is shown with the peak still 0.5ppm shifted compared to the

peak of *closo*-^{PO}Cb in step (A). In step (E), the broadened peak of *closo*-^{PO}Cb sharpened again and some side-product peak is shown at 20.7 ppm (blue star, *). And again, from steps (A) to (E), all the peaks appeared the same in our previous study during the same experiment.[1,2] Last and most interesting step (F), after the second GBE charging of the *closo*-^{PO}Cb containing solution, there showed only 4.2% *nido*-carborane generated in the solution and new peaks at 26.9 ppm and 24.2 ppm (purple star, *) appeared with each amounting to 14% and 12.6% assuming that these side products are carborane derivatives. Even though step (F) has not been exposed to UO_2^{2+}, the *nido*-carborane in the solution was shown in the form of $[UO_2 (^{PO}Cb)_2]^{2-}$, which indicates that some residue UO_2^{2+} was left in the organic layer after the back-extraction.

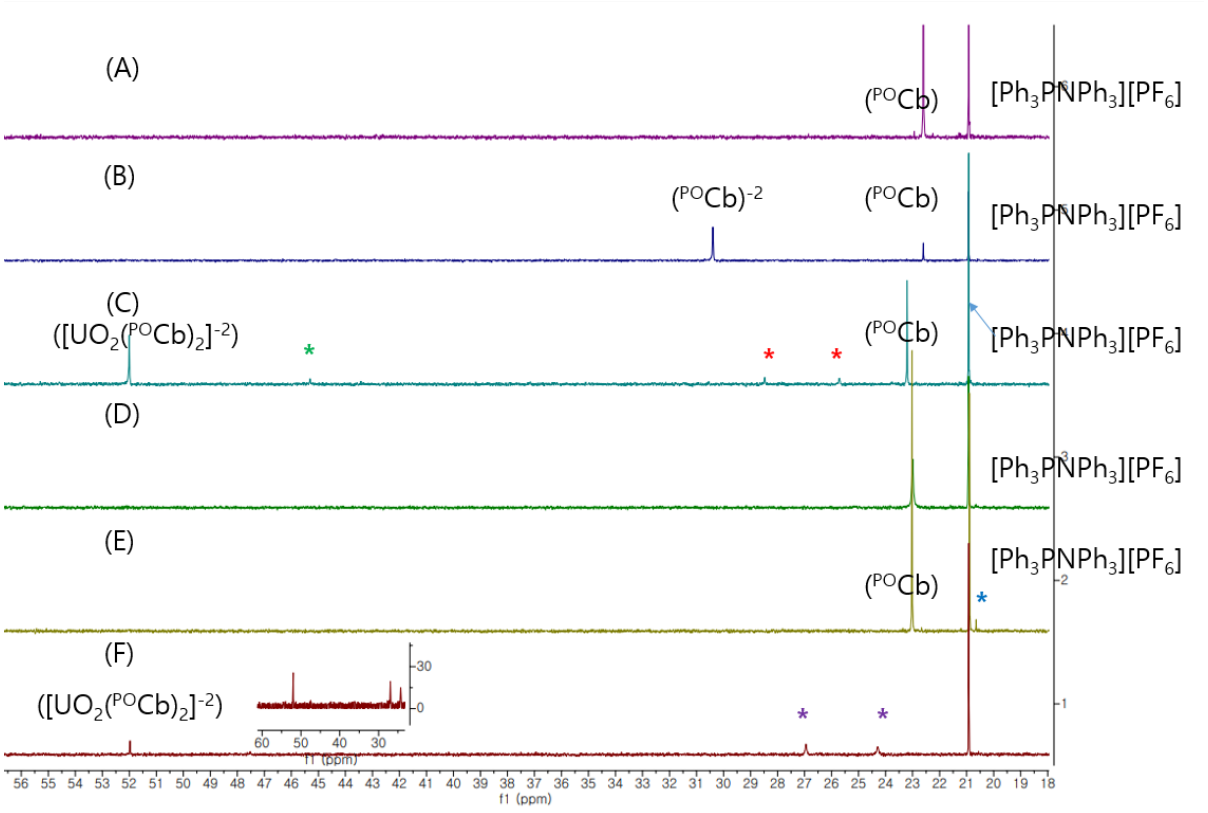

Figure 2.1. Unlocked $^{31}P\{^{1}H\}$ NMR Spectra for the electrochemical capture and release of UO_2^{2+} from a 1.25 Equiv. UO_2^{2+} metal in buffered aqueous solution (pH =5.4). Unlocked $^{31}P\{^{1}H\}$ NMR spectrum of (A) Initial **1** and $[Ph_3PNPPh_3][PF_6]$ in DCE. (B) DCE layer following GBE charging generates the reduced $[^{PO}Cb]^{2-}$ and some residual **1**. (C) DCE layer following the selective UO_2^{2+} capture from the aqueous layer containing $UO_2(NO_3)_2(THF)_2$ in 0.5 M NaOAc buffer (pH = 5.4) (D) DCE layer following GBE discharging (E) following UO_2^{2+} release by mixing with fresh NaOAc buffered solution (0.1 M) after 15 h and revealing the free carborane **1** (major), as well as an unknown by-product marked by a blue star. (F) DCE layer following GBE charging a second time with the extracted organic layer of DCE from the previous step.

This result indicates that there have been some UO_2^{2+} in the DCE layer that hasn't been gotten rid of during back-extraction. This result coincides with our previous study that back-extracted UO_2^{2+} amount in the aqueous layer was lower than expected[1] meaning some UO_2^{2+} stayed in the organic layer. Another thing to highlight is that something is interfering with the *closo*-^{PO}Cb to be reduced again. The cause can be due to the side products in the solution (which has the possibility that could not be shown $^{31}P\{^{1}H\}$ NMR) or could be the 0.5ppm shifted *closo*-^{PO}Cb forming a new adduct that is hampering reduction.

2.2.3. Method (II): Electrolysis without metal in buffer solution (pH= 5.4)

The next conducted experiment was the GBE electrolysis with NaOAc buffered solution (pH = 5.4) without uranyl. This experiment was conducted to determine whether UO_2^{2+} has a part in hampering *closo*-^{PO}Cb to being reduced a second time. **(Figure 2.2)**

In step (C), the *nido*-^{PO}Cb disappears and shows 2 different peaks at 28.5 ppm and 25.8 ppm (red star *) corresponding to [Bu_4N][^{PO}Cb H].[1] These peaks have been confirmed that its structure is [Bu_4N][^{PO}Cb H] in our previous report. In the same step, peak at 45.3ppm as unknown side product appeared like step C method I. Step (D) revealed a very broad resonance at 24.2 ppm at *closo*-^{PO}Cb peak. (E) the *closo*-^{PO}Cb showed sharp again (major). In step (F-1) a broad peak at 25ppm is shown and in (F-2) new peaks at 27 ppm and 24.5 ppm are shown. **(Figure 2.2)** After the *Closo*-^{PO}Cb has been charged once, the organic layer was mixed with a buffer solution (pH = 5.4) without uranyl. All the peaks that appeared in steps (A) to (D) of method **(I)** appear the same in this method **(II)**. (Except the peaks that formed with UO_2^{2+}).

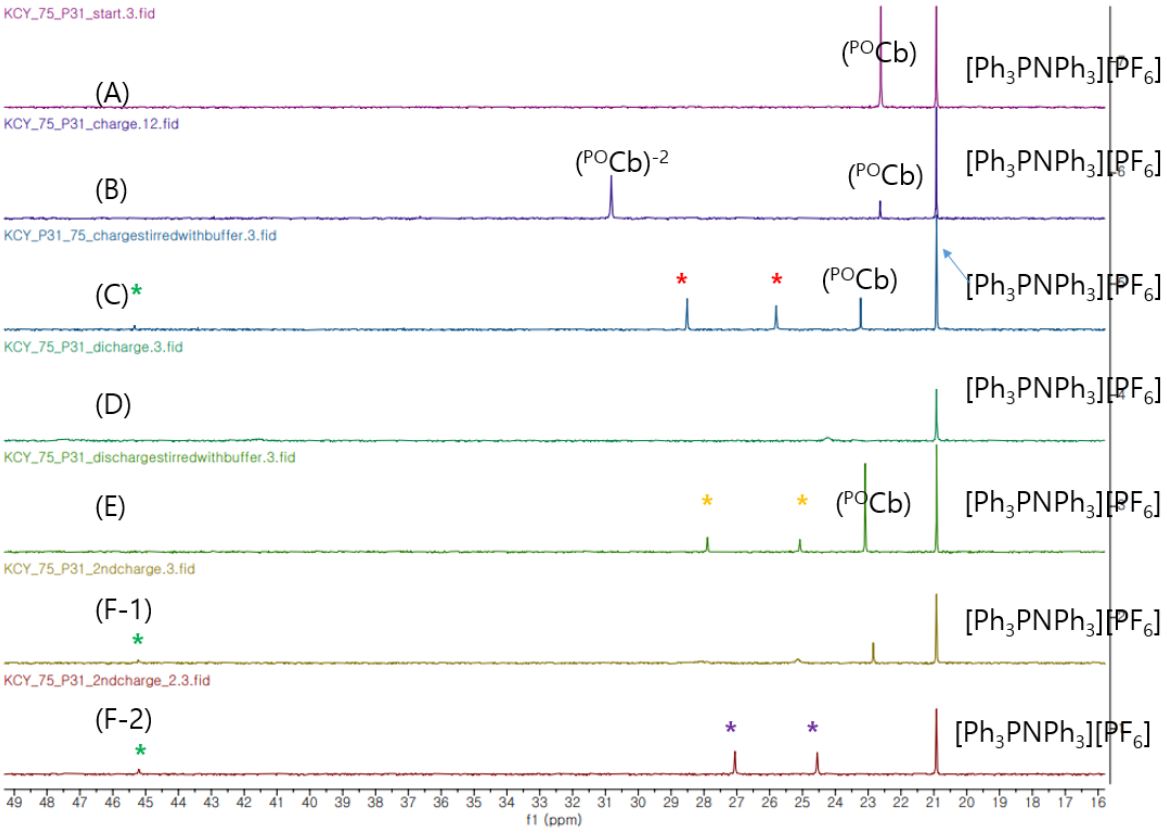

Figure 2.2 Unlocked $^{31}P\{^{1}H\}$ NMR spectra for the electrochemical from a buffered aqueous solution. (pH=5.4) Unlocked $^{31}P\{^{1}H\}$ NMR spectrum of (A) Initial **1** and $[Ph_3PNPPh_3][PF_6]$ in DCE. (B) DCE layer following GBE (C) DCE layer after 1.5 h mixing with the aqueous layer of 0.5 M NaOAc buffer (pH = 5.4) (D) DCE layer following GBE discharging (E) DCE layer mixing with fresh NaOAc buffered solution (0.1 M) after 15 h and revealing the free carborane **1** at 23ppm (major). (F-1) the DCE layer following GBE charging to a SOC of 30%, a broad peak at 25ppm (F-2) the DCE layer following GBE charging to an additional SOC of 30%, new peaks at 27 ppm and 24.5 ppm is shown

Notably, the blue starred peak that showed in method (I), step (E) at 20.7 ppm does not show in this method **(Figure 2.3).** As these side products were previously shown in method **(I),** we may conclude that the side products were formed by the buffer solution. In step (C), we also observed *closo*-^{PO}Cb shifting left about 0.5 ppm like method (I) after being exposed to the buffer solution. In step (E), the side products shown at red star ($[Bu_4N][\ ^{PO}Cb\ H]$) seem like shifted to orange starred peaks *, 27.9 ppm, and 25.0 ppm, respectively. What is surprising is that after the second charge of the **1** solution (**Figure 2.3**, step F-1), the **1** amount in the solution decreased but does not show any reduced product, a *nido*-^{PO}Cb peak.

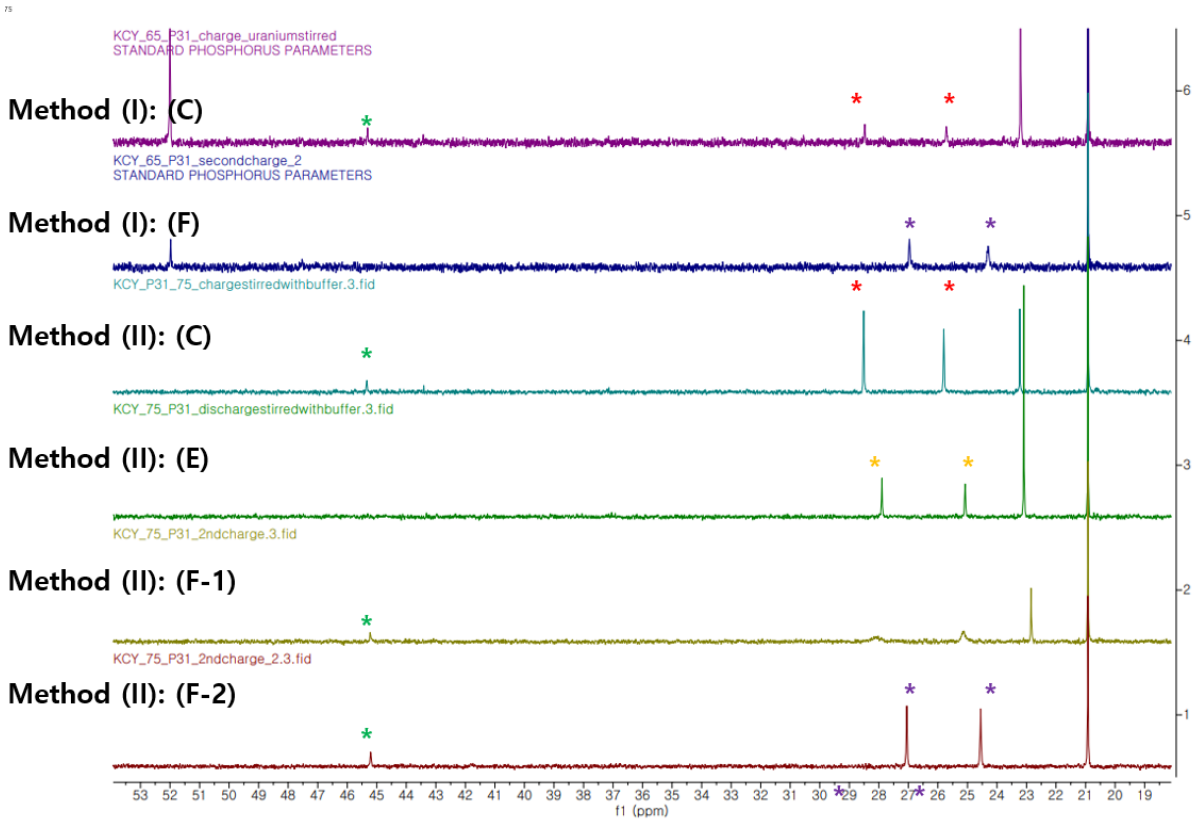

Figure 2.3 Unlocked ^{31}P $\{^{1}H\}$ NMR Spectra of Method I and Method II reassembled.

Because the second charge curve (step F) was conducted under the **method of (I)** was drastically changed **(Figure 2.4)**, we feared that this drastic change curve means charging the solution with too much current resulting in unwanted side products. Therefore, to prevent the charge curve from showing drastic change, we first applied part of the GBE charge to a SOC of 30% (**Figure 2.2** F-1, **Figure 2.5**), then applied another additional GBE charge to a SOC of 30% resulting total charge to a SOC of 60%.(**Figure 2.2** F-2). The charge curve for **Figure 2.2** F-1 showed a normal charge curve **(Figure 2.5)** whereas **Figure 2.2** F-2 showed a drastic curve change in the graph**(Figure 2.17)** like **Figure 2.4** which might have resulted in some

unwanted side products. The new peaks shown (**Figure 2.2** F-2) at 27 ppm and 24.5 ppm is possible that it is caused by unwanted side reaction due to applying too much coulomb charge.

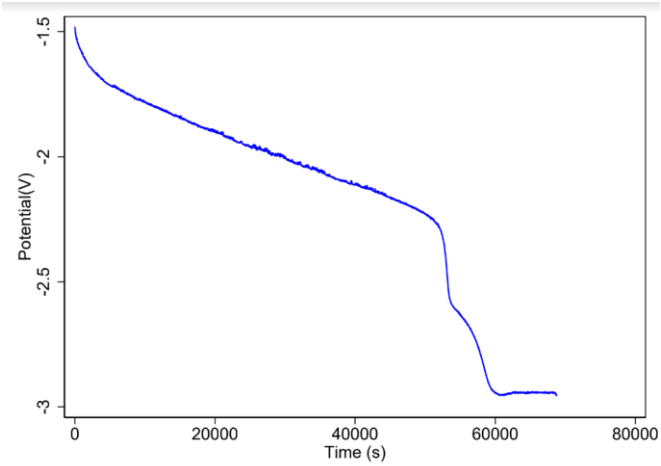

Figure 2.4. Charging Curve for the Electrochemical Capture of UO_2^{2+} of Method (I), Step (F). A charging current of -104.9 μA was applied for a total of -9.06 C of charge transferred, resulting in a 75% SOC after 24 h assuming 100% coulombic efficiency.

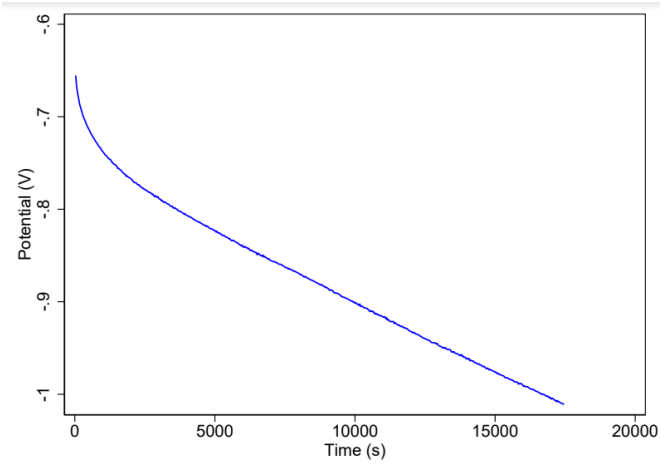

Figure 2.5 Charging Curve for the Electrochemical Capture of UO_2^{2+} . (Method II, F-1) A charging current of -104.9 μA was applied for a total of -9.06 C of charge transferred, resulting in a 75% SOC after 24 h assuming 100% columbic efficiency.

In conclusion, the side products at 27ppm and 24.5ppm that are shown in condition(I) and (II) after second charging is caused by applying too much charge(coulomb) applied, therefore it is irrelevant to the product of **1** reduced in an undesired way. The side product shown at peak 20ppm in method (I) is not shown in condition(II), so it can also be excluded as one of the factors that cause reduction hindrance. Previously we attributed the broadness of the *closo*-^{PO}Cb at a peak of 23 ppm post oxidation to an adduct of $UO_2^{2+}$with *closo*- ^{PO}Cb.[1] However, since method (II) did not contain any UO_2^{2+} but we still observe a broad peak, it is hard to say that the broad peak is caused by an adduct of $UO_2^{2+}$with **1**

2.2.4 Method (III): Electrolysis without UO_2^{2+} in water

After the *closo*-^{PO}Cb has been charged once, the DCE layer was mixed with DI water and extracted. In step C, there showed no side products (red stars, *green star *), that occurred in the method I and method II. Also, it seems like the $[^{PO}Cb]^{2-}$ peak shifted to the left after exposing the organic layer to water (pink star *) Not to mention that the *closo*-^{PO}Cb peak shifted to the left. In step D, the *closo*-^{PO}Cb peak becomes broad, barely hard to see in the spectra. After discharging the organic solvent was stirred with water for 15 hours and it showed a side product at 31.2ppm(yellow star *) (step E). No further charge has been conducted since the organic solvent was lost during the transfer to another vial. **(Figure 2.6)**

After stirring it does not show the side products produced by buffer solution(red stars, *), at 25.8ppm and 28.5ppm. that these side products were caused by acidity in the buffer solution (pH 5.4). This indicates that it is a side product produced by the buffer solution and **1.**

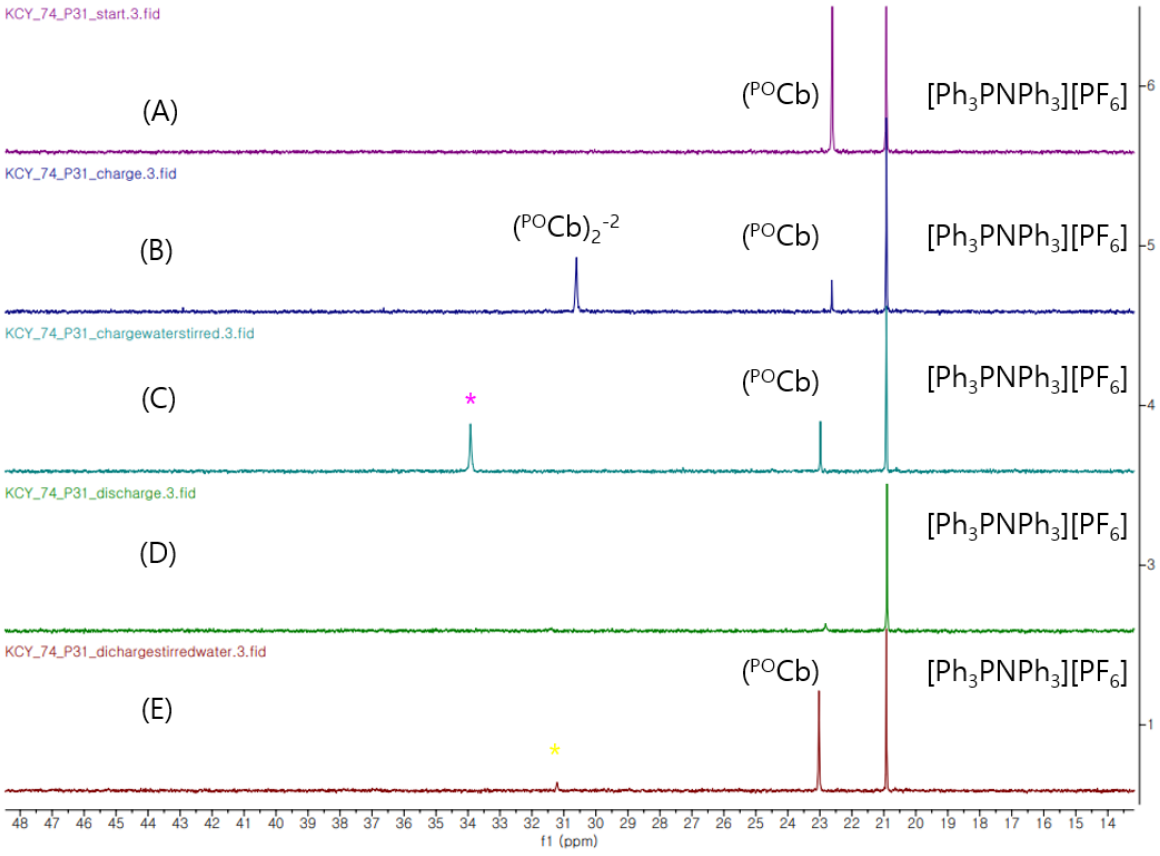

Figure 2.6 Unlocked $^{31}P\{^{1}H\}$ NMR spectra for the electrochemical from an Aqueous Solution(without any buffer or UO_2^{2+}). Unlocked $^{31}P\{^{1}H\}$ NMR spectrum of (A) Initial unlocked $^{31}P\{^{1}H\}$ NMR spectrum of **1** and [Ph$_3$PNPPh$_3$][PF$_6$] in DCE. (B) DCE layer following GBE charging generates the reduced [^{PO}Cb]$^{2-}$ and some residual **1**. (C) DCE layer following mixed with the aqueous layer containing DI water (D) DCE layer following GBE discharging revealing a very broad resonance at 23 ppm (E) DCE layer followed by mixing with DI water not buffer solution after 15 h.

Because **1** shifts left to about 0.5ppm after exposing it to aqueous buffer solution as resulted in all the previous conditions (I, II, III), we assumed that it is due to the water or acid-forming

adduct with *closo*-^{PO}Cb in the solution. In order to find out what is causing the shift *closo*-^{PO}Cb, we stopped using buffer solution whose pH is acidic enough (pH = 5.4) and used less acidic water. The shift of *closo*-^{PO}Cb is still moved to the left even though the shift change was a little less than previous methods (I, II) which indicates that the shift is likely caused by water and *closo*-^{PO}Cb **(Figure 2.7).**

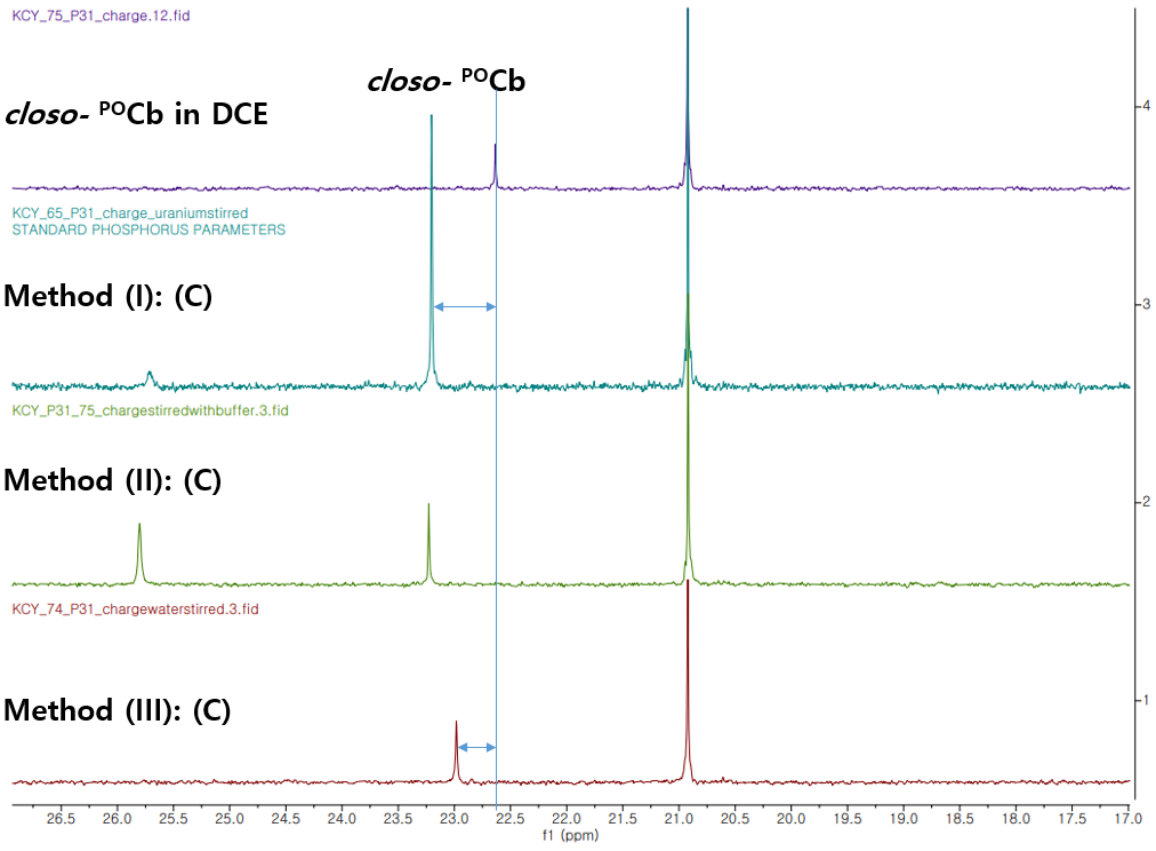

Figure 2.7. Unlocked $^{31}P\{^{1}H\}$ NMR Spectra of **Step C** of Method I, Method II, and Method III reassembled.

Further study has been conducted to see the shift according to acidity of water layer. *Closo*-^{PO}Cb stirred with different acid water solution changes shift to left about 0.3ppm, 0.8ppm,

19.1ppm each as the acidity increased. We were able to conclude that the more acidic the condition is, the more downfield shifted the chemical shift of *closo*-^{PO}Cb goes **(Figure 2.8)**.

A protonated carborane was synthesized and isolated by stirring with 1eq. of **1** with 1 eq. of Hbarf in DCE solvent, which showed same chemical shift as 19.1 ppm shifted signal. The protonated structure of the carborane was confirmed by XRD. **(Figure 2.9)**

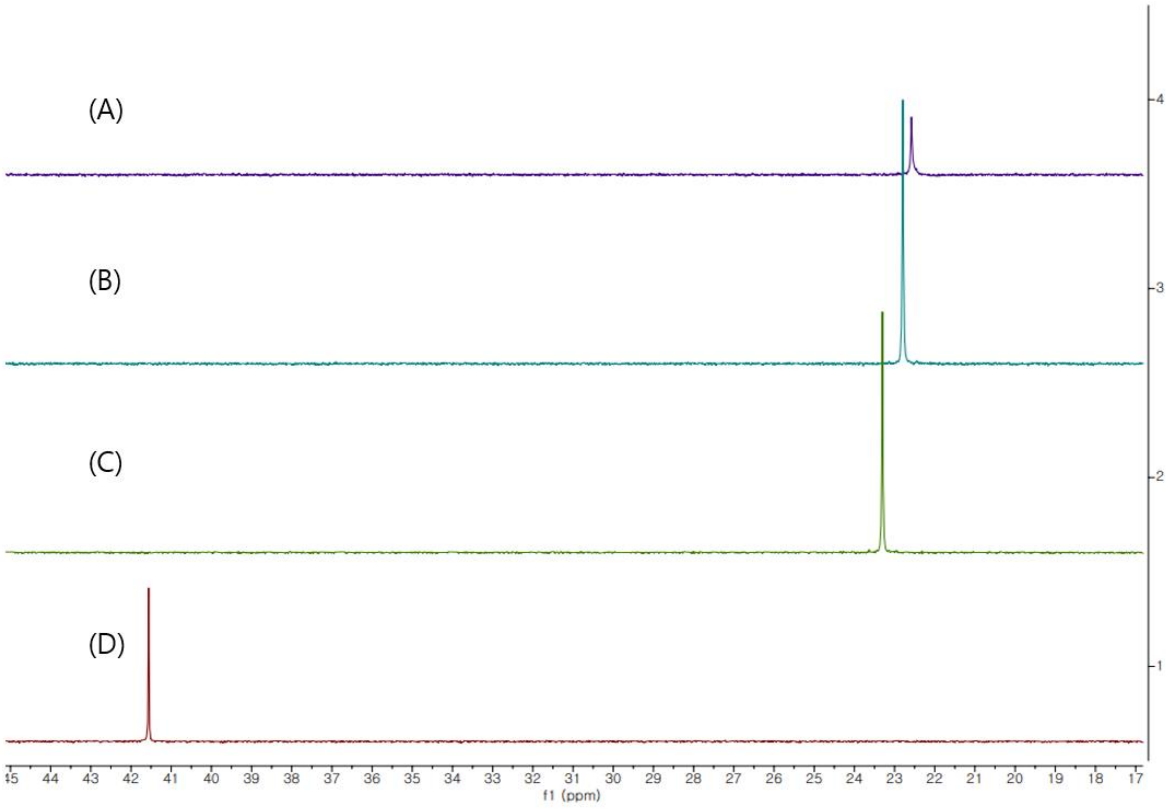

Figure 2.8 Unlocked $^{31}P\{^{1}H\}$ NMR Spectra for *closo*- ^{PO}Cb in a different acidic condition in DCE solvent (a) in DCE solvent, 22.5ppm (b) stirred overnight with water and extracted DCE layer, 22.8ppm (c) stirred overnight with aqueous nitic acid (pH = 0) solution and

extracted DCE layer, 23.3ppm (d) stirred overnight with Hbarf (Brookhart's acid) in DCE layer, 41.6ppm

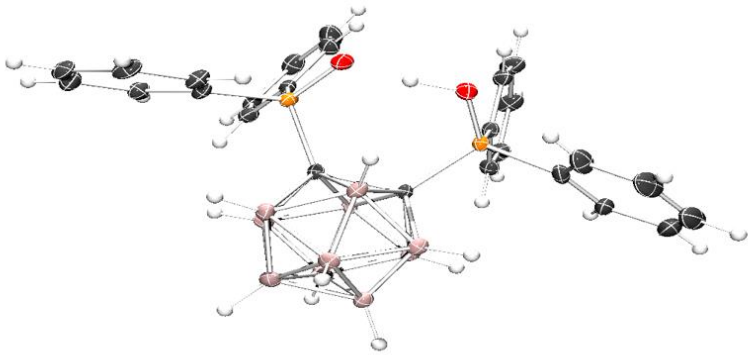

Figure 2.9 Solid-state molecular structure of protonated **1([**^{PO}CbH][B (PhF_5)$_4$], B (PhF_5)$_4$$^{-1}$(counter anion) and all co-crystallized solvent(DCE) molecules are omitted for clarity.O_1-H_1 1.062, O_2-H_1 1.325 2.364, P-P3.726, C-C 1.715

2.2.5 Method (VI): Electrolysis without water/buffer/ uranyl

Exploring without any water stirred (nor buffer) shows that *nido*-^{PO}Cb and *closo*-^{PO}Cb are moderately recovered and can be reused again since the total amount of nido- and closo Cb of the carborane after the second charge is about 0.03671mmol according to the internal standard in ^{31}P, which is about 72% of the initial amount of initial *closo*-^{PO}Cb and regenerated 40.4% of *nido*-^{PO}Cb([^{PO}Cb]$^{2-}$). Some minor peaks have been detected around 40 ppm after the second charge but none of them overlaps with previous side products. We can conclude that this second charge is working better in forming a decent amount of *nido*-^{PO}Cb.

(Figure 2.10) Therefore, we can say that once the DCE layer is exposed to some sort of aqueous solution, it is hard to gain *nido*-^{PO}Cb after the second charge.

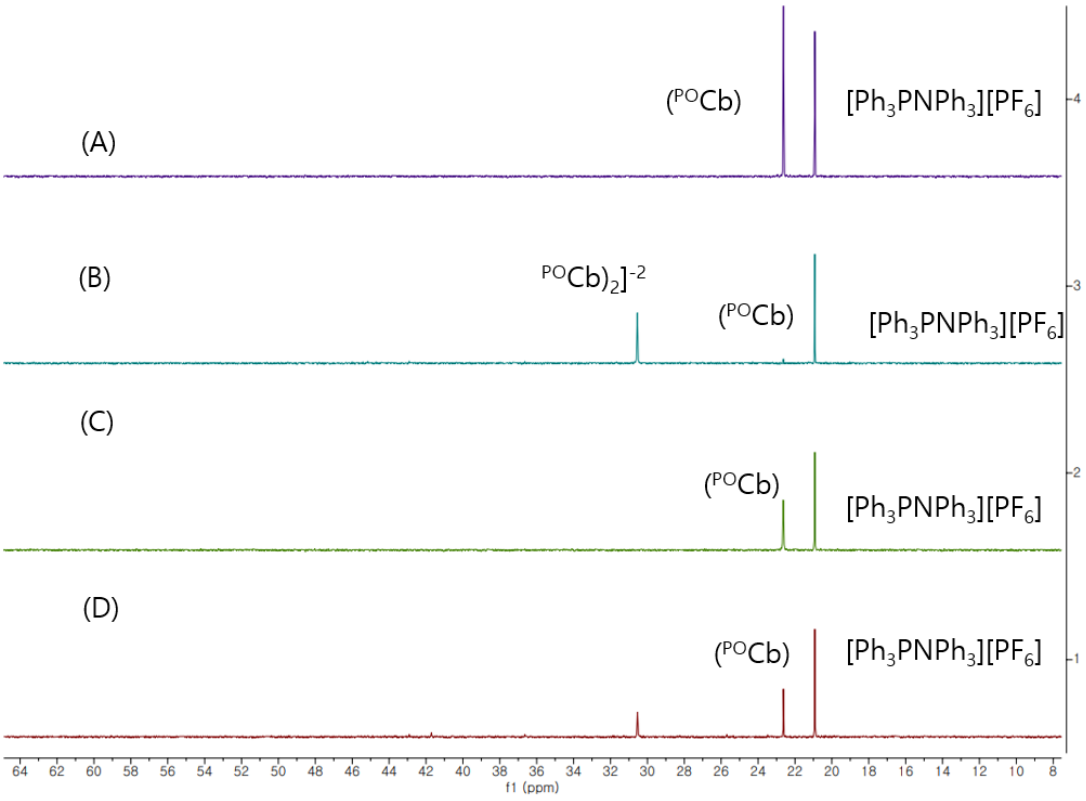

Figure 2.10 Unlocked $^{31}P\{^{1}H\}$ NMR Spectra for the Electrochemical without aqueous extraction/ uranyl /buffer solution. Unlocked $^{31}P\{^{1}H\}$ NMR Spectra of (A) Initial **1** and $[Ph_3PNPPh_3][PF_6]$ in DCE. (B) DCE layer following GBE charging generates the reduced [^{PO}Cb]$^{2-}$ and some residual **1**. (C) DCE layer following GBE discharging. (D)DCE layer following GBE charging generates the reduced [^{PO}Cb]$^{2-}$ and some residual **1**.

A factor hindering the reduction of *closo*-^{PO}Cb might be side products in the DCE layer. As we compare all the side products formed at step E of Method (I, II, III, IV) which is just before we charge the second time, there are no common side products in the solution that we

can say that it is hindering the charging. All the methods except method IV show in common of the product/peak are shifted *closo*-^{PO}Cb peak. (**Figure 2.11**). Therefore, we suspect that this species is what has been causing side reactions to hinder *closo*-^{PO}Cb reduction to *nido*-^{PO}Cb.

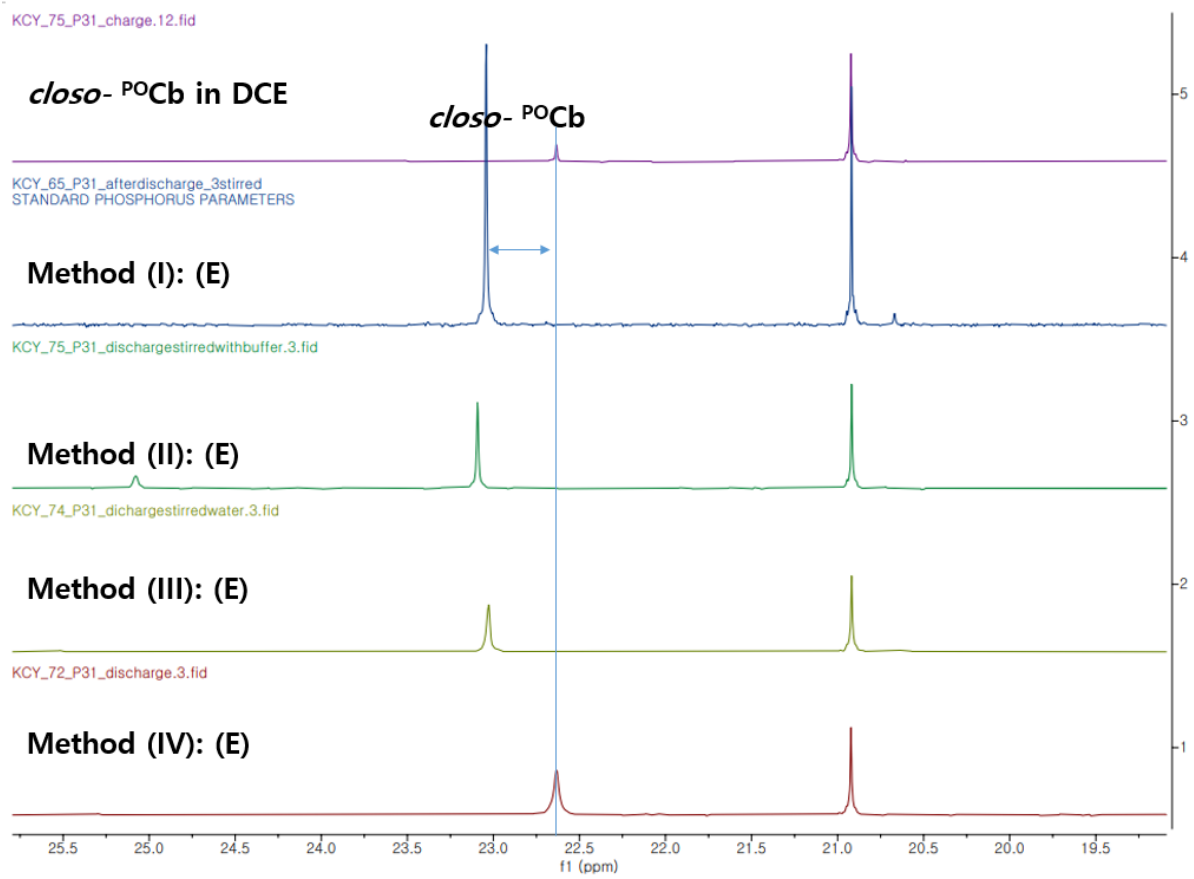

Figure 2.11 Unlocked $^{31}P\{^{1}H\}$ NMR Spectra of *closo*-^{PO}Cb at **Step E** of Method I, Method II, Method III, and Method IV reassembled.

2.3 Summary

In summary, we explored the potential of reusing **1** for another capture of metal after capturing UO_2^{2+} once. By comparing differently conditioned GBE electrolysis, we were able to exclude side products that are irrelevant in the hindrance of the second reduction of **1** and

found out the only common peak exhibited on ^{31}P before the second reduction with GBE is the **1** peak shifted left to 0.5ppm. This could lead to an unwanted reaction for **1** to form side product, not to *nido*-carborane. When it is not exposed to any aqueous solution, the **1** peak does not shift and shows good reduction, about 40% in reduced form compared to the initial amount. However, when it is reduced to **1** shifted state, the amount of *nido*-form of **1** shows from about 8% to 0%. Therefore, it is likely that the *nido*- ^{PO}Cb is causing the second charge to not occur.

The biphasic capture is essential since the UO_2^{2+} is in water and our carborane dissolves in the organic solvent. Therefore, this study gives some glimpses of finding a procedure that recycles the carborane we use to capture UO_2^{2+}. This is an important starting point since reusing **1** is important from an economic and environmental perspective. We note a loss of *ca.* 20 % of combined carborane resonances (**1** and ^{PO}Cb $^{2-}$) following charging and relative to the starting solutions and internal standard, perhaps due to ill-defined electrochemical side reactions which are not shown in ^{31}P NMR spectroscopy.

2.4 Experimental

General Considerations. All manipulations were performed under an atmosphere of dry, oxygen-free N_2 within an MBraun glovebox (MBRAUN UNIlab Pro SP Eco equipped with a -35 °C freezer), or by standard Schlenk techniques. Pentane, hexanes, Et_2O, DCM, DCE and THF (inhibitor-free) were dried and degassed on an MBraun Solvent Purification System and stored over activated 4 Å molecular sieves. Celite® and 4 Å molecular sieves were dried at 250 °C under a dynamic vacuum (<0.1 Torr) for 24 h before use. All other reagents were obtained from Sigma-Aldrich, Fisher Scientific, or VWR and used without further purification.

Spectroscopic Measurements. NMR spectra were obtained on an Agilent Technologies 400 MHz DD2, Varian Unity Inova 500 MHz, Bruker Avance NEO 500 MHz, or a Varian 600 MHz spectrometer, and referenced to residual solvent. Chemical shifts (δ) are recorded in ppm and the coupling constants are in Hz. J. Young air-tight adaptors were used for air- and water-sensitive compounds. All measurements were performed on the recrystallized product. All stock solutions and dilutions were prepared by mass.

Experimental Conditions Two-electrode galvanostatic bulk electrolysis (GBE) was performed in an argon glovebox utilizing a two-compartment H-cell with a glass frit separator, a stir bar in each compartment, and reticulated vitreous carbon (RVC) foam electrodes for both the working and counter electrodes. The RVC foam electrodes consisted of a ~5 cm steel rod inserted into 100 PPI Duocel® RVC foam core (length ~3 cm; diameter ~3 mm), with a tapped bore (length ~5 mm; diameter ~2 mm), which was filled with molten gallium to fuse the steel connector to the RVC foam. The RVC electrodes were rinsed with acetone and dried before use. The Ketjenblack used was dried for 48 h in a 175 ^{o}C oven and ground in a glass mortar and pestle under an inert atmosphere before use.[1]

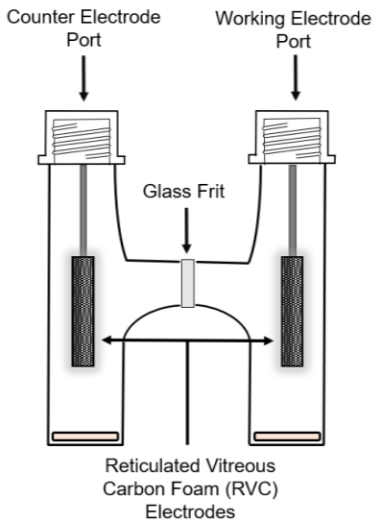

Figure 2.12 H-Cell Design. Schematic of the two-compartment H-cell used for the biphasic electrochemical separation and recovery of UO_2^{2+}.

Experimental Methods

Reduction (Charging) 1: The counter compartment consisted of 300 mg of Ketjenblack suspended in 8 mL of a 0.1 M solution of $[Bu_4N][PF_6]$ in DCE. The working compartment consisted of **1** (**X mg**, 1.0 equiv) and $[Ph_3PNPPh_3][PF_6]$ (**Y mg** , 0.5 equiv) dissolved in 6 mL of a 0.1 M solution of $[Bu_4N][PF_6]$ in DCE. An initial 31P{1H} NMR spectrum was obtained from the DCE layer. A charging current of **Z** μA with a **W** charge cutoff was utilized, resulting in a ca. 75% SOC after 24 h assuming 100% columbic efficiency. Upon completion, the working compartment solution was analyzed by ^{31}P $\{^1H\}$ NMR spectroscopy to reveal the

formation of $[^{PO}Cb]^{2-}$ with some remaining **1**. Based on $[Ph_3PNPPh_3]$ $[PF_6]$, the amount of $[^{PO}Cb]^{2-}$ was determined to be **Q** (% yield)*. The working compartment solution was then removed from the H-cell and placed in a 20 mL vial for subsequent selective UO_2^{2+} capture chemistry.

Condition	X (mg (mmol))	Y (mg (mmol))	Z (uA)	W (C)	Q (mmol (%))
I	34.1(0.06261l)	21.3 (0.03116)	104.9	9.06	0.0433 (65. 6)
II	34.1(0.06261l)	20.2 (0.029552)	104.9	9.06	0.0380 (68.6)
III	34.1(0.06261l)	20.4 (0.029844)	104.9	9.06	0.0376 (69.2)
VI	34.6(0.063534)	20.4(0.029844)	106.4	9.19	0.0380 (68.6)

Table 2.1 Experimental quantity in conditions from (I) to (IV)

*yield compared with the initial amount determined by ^{31}P NMR spectroscopy and internal standard

Selective UO2 2+ Capture: Crystalline $UO_2(NO3)_2(THF)_2$ dissolved in 5mL of 0.5 M NaOAc buffered solution (pH = 5.4) resulting in a bright yellow stock solution**.(Method I)*** A 5 mL aliquot of the stock solution (1.25 equiv) was added dropwise without stirring to the DCE solution containing the electrochemically reduced $^{PO}Cb^{2-}$. After addition, the mixture was allowed to stir for 1.5 h, resulting in a bright yellow organic phase and a transparent aqueous phase. Stirring was discontinued and the organic and aqueous phases were separated using a small separatory funnel. A 0.5 mL aliquot was taken from the yellow DCE layer and transferred to an NMR tube. An unlocked ^{31}P $\{^1H\}$ NMR spectrum was collected indicating the formation

of $[UO_2(POCb)_2]^{2-}$, as well as some **1** and $[Bu_4N][^{PO}CbH]$. The NMR solution was returned to the 20 mL vial.

*This part can be skipped according to the method used, It can be changed to 5mL of NaOAc buffer solution (pH=5.4) (**Method II),** 5mL of water **(Method III),** no aqueous solution **(Method IV)**

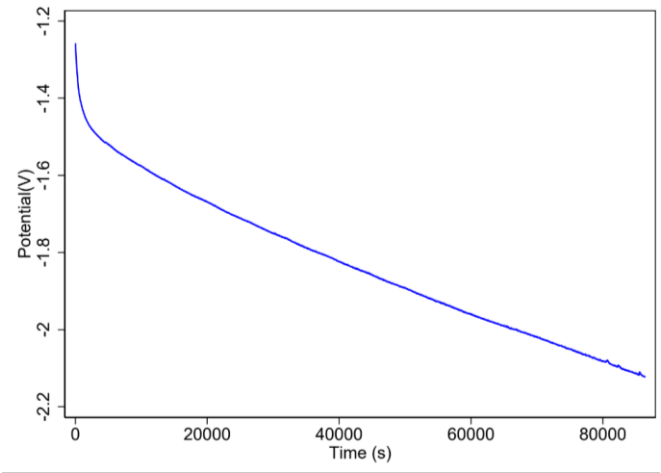

Figure 2.13. Charging Curve for the Electrochemical Capture of UO_2^{2+} (Method I, B). A charging current of -104.9 μA was applied for a total of -9.06 C of charge transferred, resulting in a 75% SOC after 24 h assuming 100% columbic efficiency.

Oxidation (Discharging): The DCE layer was returned to the H-cell and GBE was used to discharge (oxidize) the carborane, initiating UO_2^{2+} release. A discharging current of **Z** μA with a **W** C charge cutoff was utilized resulting in a final SOC of ca. 0 % (; assuming 100% columbic efficiency and no loss of material during the biphasic capture)**.(Table 2.1)** Upon completion, a 0.5 mL aliquot was taken from the pale yellow DCE layer and transferred to an NMR tube. An unlocked $^{31}P\{^1H\}$ NMR spectrum was collected indicating a very broad signal

between 35–40 ppm. The NMR sample and working compartment solutions were combined and placed in a 20 mL vial for subsequent release chemistry

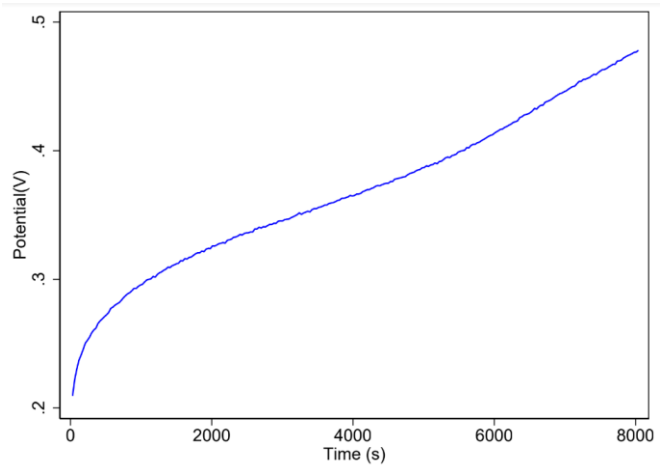

Figure 2.14. Discharging Curve for the Electrochemical Release of UO_2^{2+} (Method I, D). A discharging current of 107.1 µA was applied for a total of ca. 9.25 C of charge transferred, resulting in a 0% SOC after 24 h assuming 100% columbic efficiency.

UO_2^{2+} recovery: The 20 mL vial containing the electrochemically discharged DCE solution was equipped with a stir bar and a 5 mL solution of 0.1 M NaOAc buffer (Method I,II) *was added dropwise to it. The mixture was allowed to stir for 15 h, resulting in a bright-yellow aqueous phase and a colorless organic layer. A 0.5 mL aliquot was taken from the colorless DCE layer and transferred to an NMR tube. An unlocked $^{31}P\{^{1}H\}$ NMR spectrum was collected indicating the clean formation of **1**, $[Ph_3PNPPh_3][PF_6]$.

*This part can be skipped according to the method used, It can be changed to 5mL of water **(Method III),** no aqueous solution **(Method IV)**

Reduction (Charging) 2:

The table below demonstrate quantities of carborane and conditions of electrolysis. An **X** mmol of **1** was determined by ^{31}P {^{1}H} NMR spectroscopy and internal standard. A charging current of **Z** μA with a **W** charge cutoff was utilized, resulting in a ca. 30% SOC assuming 100% columbic efficiency. Upon completion, the working compartment solution was analyzed by ^{31}P {^{1}H} NMR spectroscopy to reveal the formation of [$^{PO}Cb]^{2-}$ with some remaining **1**. Based on [Ph_3PNPPh_3] [PF_6], the amount of [$^{PO}Cb]^{2-}$ was determined to be **Q** (% yield)*.

Condition	**X mmol**	**Z (uA)**	**W (C)**	**Q (mmol (%))**
I	0.05234	87.6	7.57	0.00529 (8.0)
II	0.03163	104.9 104.9	1.8 1.8	0 0
IV	0.04536	106.4	2.62, 3.4	0.00596 (11.8) 0.02059(40.6)

Table 2.2 Experimental quantity in conditions from (I) to (IV)

*yield compared with the initial amount determined by ^{31}P NMR spectroscopy and internal standard

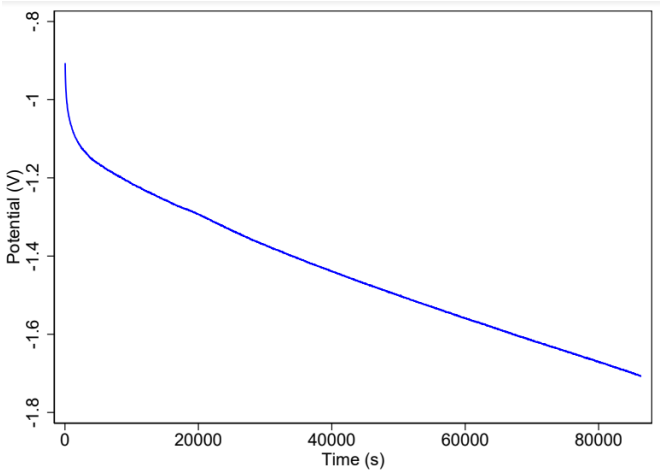

Figure 2.15. Charging Curve for the Electrochemical Capture of UO_2^{2+} (Method II, B).

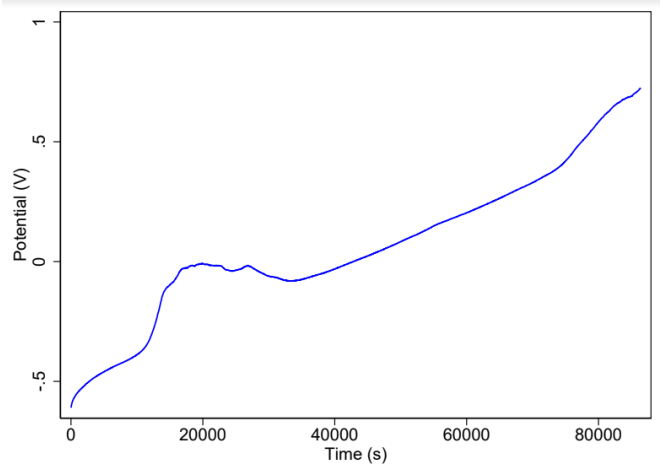

Figure 2.16. Discharging Curve for the Electrochemical Release of UO_2^{2+}(Method II, D).

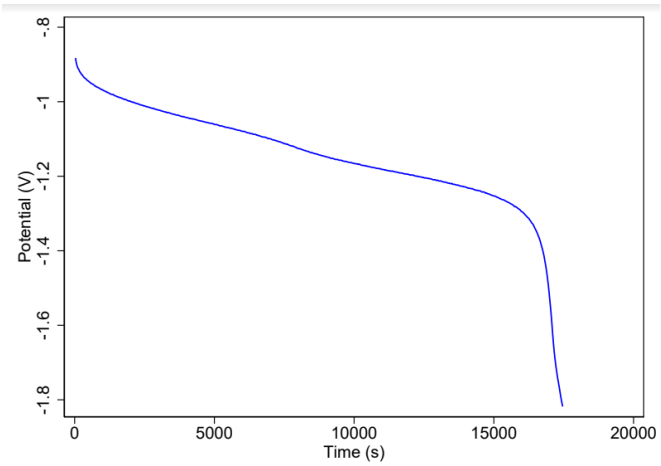

Figure 2.17. Charging Curve for the Electrochemical Capture of UO_2^{2+} (Method II, F-2)

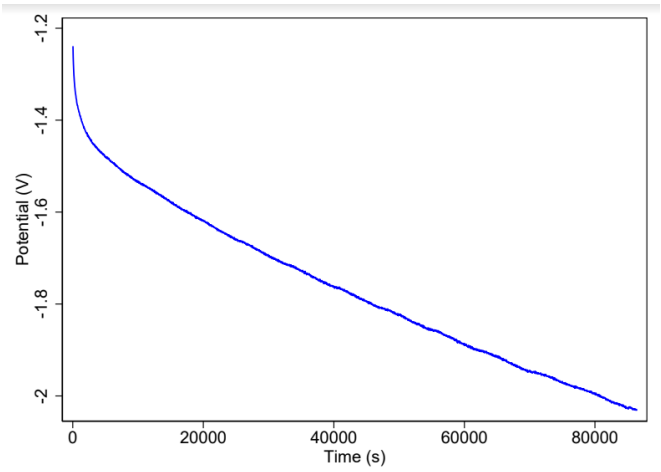

Figure 2.18 Charging Curve for the Electrochemical Capture of UO_2^{2+} (Method III, B).

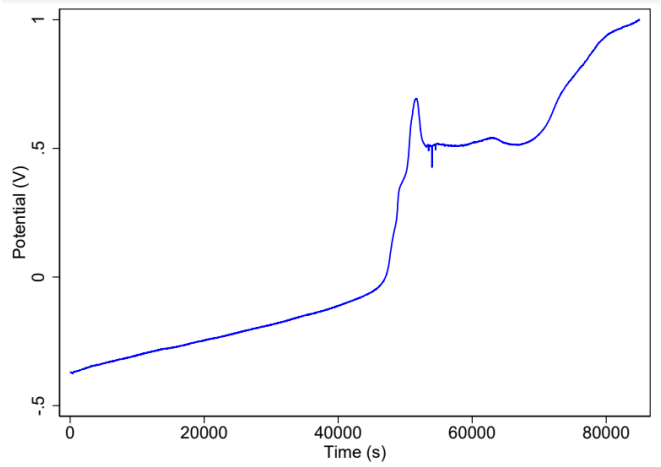

Figure 2.19. Discharging Curve for the Electrochemical Release of UO_2^{2+} (Method III, D).

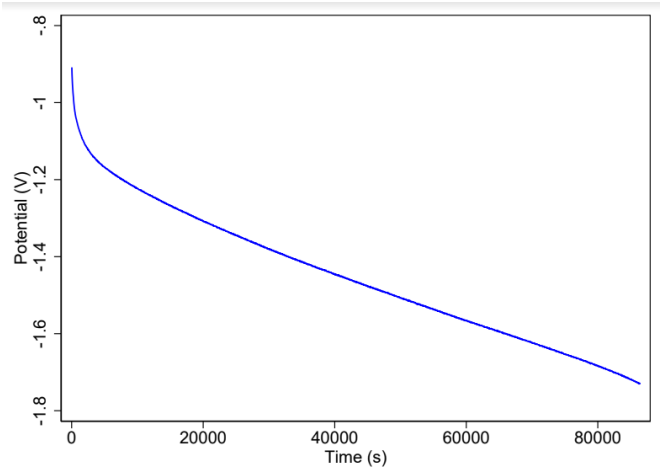

Figure 2.20. Charging Curve for the Electrochemical Capture of UO_2^{2+} (Method IV, B).

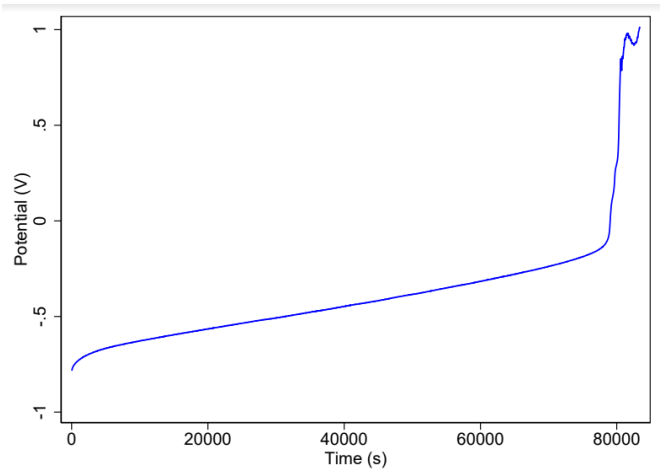

Figure 2.21. Discharging Curve for the Electrochemical Release of UO_2^{2+} (Method IV, D).

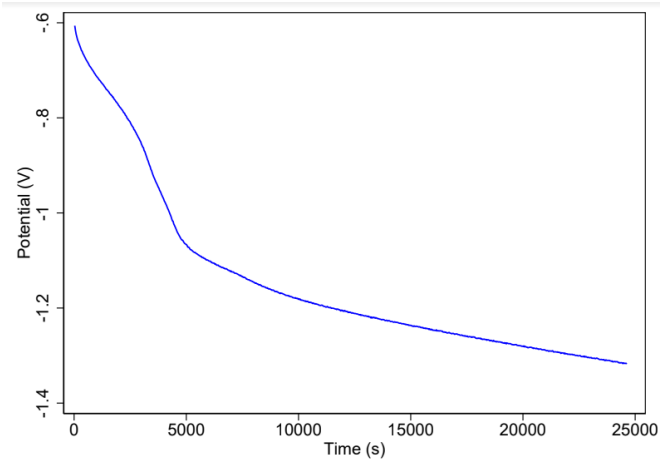

Figure 2.22. Charging Curve for the Electrochemical Capture of UO_2^{2+} (Method VI, F-1)

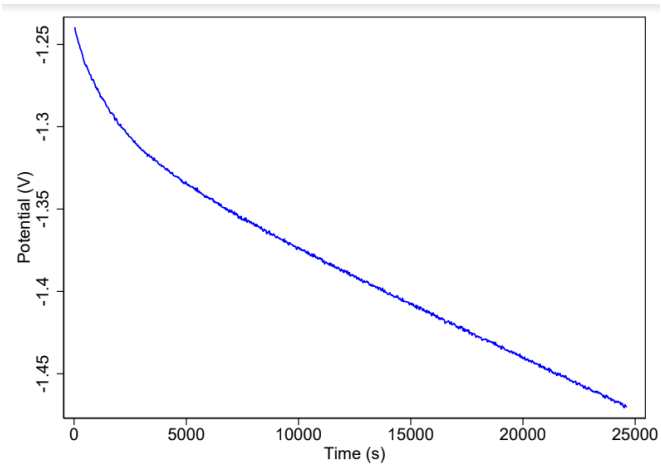

Figure 2.23. Charging Curve for the Electrochemical Capture of UO_2^{2+}. (Method VI, F-2)

Synthesis of protonated 1 ([^{PO}CbH][B (PhF_5)$_4$])

27.2mg of **1** was mixed with 0.5mL of DCE and was stirred at -76ºC for 3 minutes. Then the 50mg of Hbarf in 0.5mL of DCE solution (slightly pink colored) was added and mixed for overnight. The solution was filtered through celite. Single crystals suitable for XRD studies were obtained by vapor diffusion of pentane over a saturated $CDCl_3$ solution of **([^{PO}CbH][B (PhF_5)$_4$]** at room temperature. Yield was not gained due to water residue.**^{1}H NMR** (400 MHz, $CDCl_3$): δ 7.84 (broad, 8H, Ph), 7.70 (broad, 4H, Ph), 7.54 (broad, 8H, Ph), Carborane B-H, PO-H resonance were too broad to be observed, **^{11}B {^{1}H} NMR** (128 MHz, $CDCl_3$): δ 4.54; -5.45; -8.82; -16.72**. ^{31}P {^{1}H} NMR** (162 MHz, $CDCl_3$): δ 41.55

2.5 References

1. Keener, M.; Hunt, C.; Carroll, T. G.; Kampel, V.; Dobrovetsky, R.; Hayton, T. W.; Ménard, G. Redox-Switchable Carboranes for Uranium Capture and Release. *Nature* **2020**, *577* (7792), 652–655.
2. Keener, M.; Mattejat, M.; Zheng, S. L.; Wu, G.; Hayton, T. W.; Ménard, G. Selective Electrochemical Capture and Release of Uranyl from Aqueous Alkali, Lanthanide, and Actinide Mixtures Using Redox-Switchable Carboranes. *Chem. Sci*. **2022**, *13 (12)*, 3369–3374.
3. Nguyen-trung, C.; Humbert, B. Hydrolysis of Uranyl (VI) in Acidic and Basic Aqueous Solutions Using a Noncomplexing Organic Base : A Multivariate Spectroscopic and Statistical Study. *Inorg. Chem.* **2011**, *No 50*, 2811–2823.
4. Pant, D. D., Handelwal D. P. The absorption and fluorescence spectra of uranyl nitrate solutions at room temperature., D.S.B. Government College, **1959**, 323–335.

Chapter 3

Lanthanide capture with redox switchable diphenyl phosphine oxide substituted *ortho*-carborane

3.1 Introduction

Lanthanides have a lot of usage in many fields such as batteries and permanent magnets, fluid cracking catalysts, and therapeutic agents.[1] Cerium (Ce) is used for glass manufacturing, Gadolinium (Gd) and Yttrium (Y) in television phosphors, and nuclear control rods, and lastly Erbium (Er), Terbium (Tb), and Europium (Eu) are commonly used in glass and porcelain tints, postage stamps.[9,10] The attention to reusing lanthanide from the PUREX processed waste stream[13] has increased to assure the stability of production and supply. Our approach for lanthanide capture and release is to utilize redox switchable **1**. After the reduction of **1**, the C-C bond ruptures, and the conformation of the Cb cage changes increasing the bite angle of the P=O donor group, which was enough to coordinate larger metals such as uranyl.[2,3] The use of **1** for uranium capture can further extend electrochemical and biphasic conditions. From the successful results we got of using the redox switchable **1** to capture uranyl, we extended this strategy of capturing uranium to different lanthanide metals. The possibility of easy capture and release of lanthanide may assist in solving the situation of the scarcity of lanthanide metals and also help us gain independence from the lanthanide source. The details will be presented in this chapter.

3.2 Results and Discussion

3.2.1 Synthesis of K_2 [^{PO}Cb]

To probe the capability of *nido*-^{PO}Cb for capturing lanthanide, we started by chemically reducing **1** to *nido*-^{PO}Cb in form of K_2[^{PO}Cb] (**2**).**(Scheme 3.1)** The K_2[^{PO}Cb] was synthesized according to the previously reported method from our group.[4] 2.7 eq. of KC_8 were added to *closo*-^{PO}Cb at −78 °C in THF solution and slowly warmed to room temperature. After stirring the solution for 30 min at room temperature, the resulting mixture was filtered through celite to remove excess KC_8 and the filtered THF solution was further purified by layering recrystallization with pentane, affording the white crystal of **2.**

Crystal structure of **2** was gained through XRD experiment. The bond length between carbon-carbon bond was 2.857 and phosphorous-oxygen was 1.487. **(Figure 3.1)**

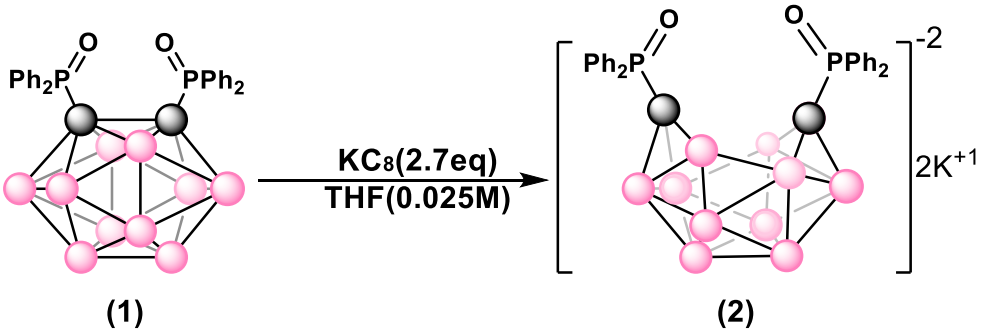

Scheme 3.1 Reduction of **1** to K_2 [^{PO}Cb] using KC_8

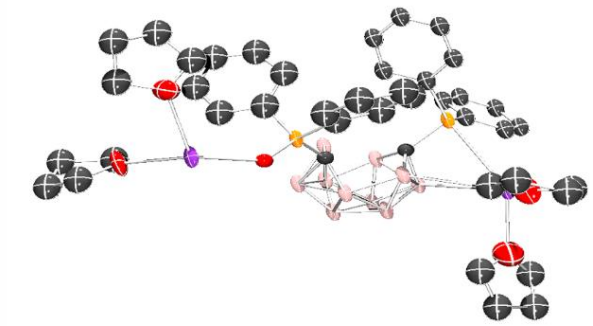

Figure 3.1 Crystal structure of $K_2[^{PO}Cb]$

3.2.2. Lanthanide coordination with *nido*-^{PO}Cb

The investigation of **2** for lanthanide capture was conducted by mixing different Ln metals complexes, $Ln(NO_3)_3THF_3$, with **2** in acetonitrile at room temperature **(Scheme 3.2)**. All $Ln(NO_3)_3THF_3$ were prepared from $Ln(H_2O)_x(NO_3)_3$.[11] After adding dropwise $Ln(NO_3)_3THF_3$ to **2** in acetonitrile solution the reaction immediately became cloudy for all the reactions, due to the low solubility of KNO_3 in acetonitrile.[5] The reaction mixture was stirred overnight and the solid was filtered through celite and the solution was dried under vacuum and recrystallized with acetonitrile then layered with pentane, ether, or hexane. The products were identified by single crystal XRD studies The **table 3.1** shows the summary of

the result of the reaction with different $Ln(NO_3)_3THF_3$.

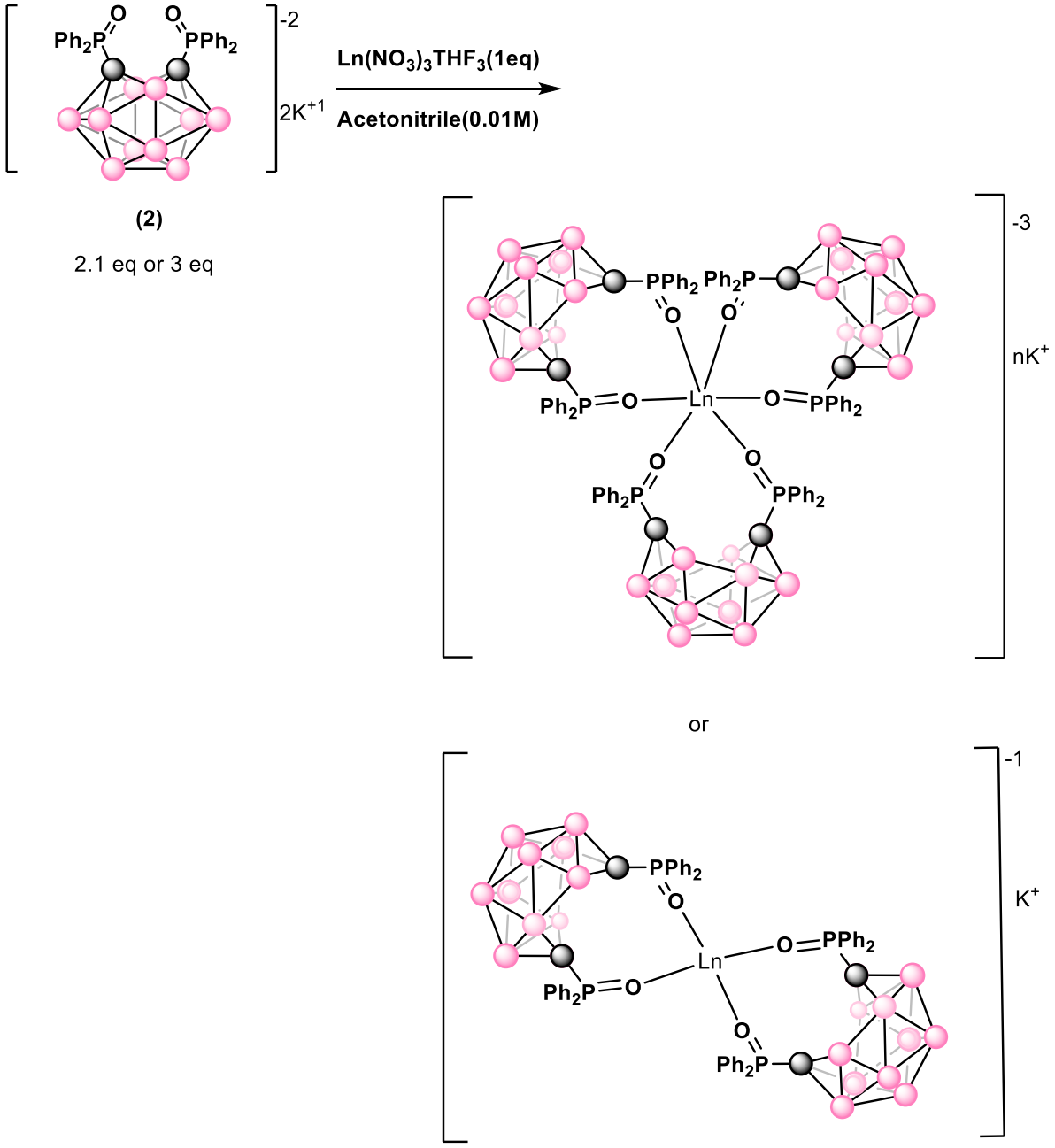

Scheme 3.2 Coordination with Lanthanide

During the reaction with $Ln(NO_3)_3THF_3$, we did not consider that **2** contained THF adducts. Therefore, less than 3 equivalent of **2** was initially added to $Ln(NO_3)_3THF_3$. We found out that **2** contained 4 THF adducts from solid-state structure, which meant that 2.1 equivalent of **2** was added during the reaction with $Ln(NO_3)_3THF_3$ for (specific metals) case. The correct 3 equivalents of **2** was added for the reaction with $Ln(NO_3)_3THF_3$ for a few (specific metals) cases.

In **table 3.1,** as the atomic number increases, the size of the lanthanide metal decreases due to the lanthanide contraction[13]. As we have reacted **2** with Ln metal in a 2.1 :1 ratio, we were able to get the crystal structure of each coordinating group and were able to determine how many *nido*-^{PO}Cb are chelating per one lanthanide metal from XRD data except Eu since it was poorly diffracting. The results showed 2 different coordinating systems. One is a 2:1 chelating group that is all charge balanced whereas, another formed a 3:1 cluster. For reaction with lanthanide metals such as Dy **(Figure 3.2)**, Eu **(Figure 3.3)** and Ce **(Figure 3.4)** that only 2.1 equiv of **2** was added, the solid-state structure indicated the product contained two **2** for each lanthanide metal. All the cluster that is chelating in with the ratio of 2:1([^{PO}Cb]: Ln), are charge balanced. However, their size and the number of ^{PO}Cb chelating to the metal doesn't seem to have a trend since Cerium is the biggest size of the lanthanide series and Tb, Ho is on the right side of the series, meaning smaller in size compared to Ce.

Atom number	58	59	60	62	63	65	66	67	68
Lanthanide types	Ce	Pr[a)]	Nd* [a)]	Sm*[a)]	Eu	Tb	Dy	Ho	Er
Number of Carborane per lanthanide metal	2	3	3	3	3	3	2	3	2
Charge balance c)	Balanced	Balanced	Balanced	Balanced	Missing more than 2K (2.5)	Missing >1 K (more than 1K)	Balanced	Missing 1 K	Balanced
C-C bond length after coordination (Å)	2.855 2.839	2.791 2.791 2.761	2.83 2.82 2.83	2.79 2.87 2.81	b)	2.811 2.609 2.826	2.848 2.849	2.790 2.873 2.790	2.864 2.872

Table 3.1 *nido*-^{PO}Cb coordinating (2.1eq) with different Lanthanide metals (1eq.)

*Nd, Sm data is gained from the previous study of Menard's group[4,7]

a) Pr, Sm, Nd was reacted with not $K_2[^{PO}Cb]$ but with $[CoCp_2^*]_2$ $[^{PO}Cb]$, reactions were done with a 3:1 eq ratio

b) Eu XRD data was not gained due to poor diffraction, therefore C-C bond was not gained

c) K amount is not fully determined due to the temperature factor.

Dysprosium (Dy) is forming a 6 coordinate cluster with 2 carboranes and 2 acetonitrile molecules.The average C-C bond length of the carboranes in a cluster is 2.848.5 Å and the total cluster has charge of -1. One potassium is around to balance the charge.**(Figure 3.2)**

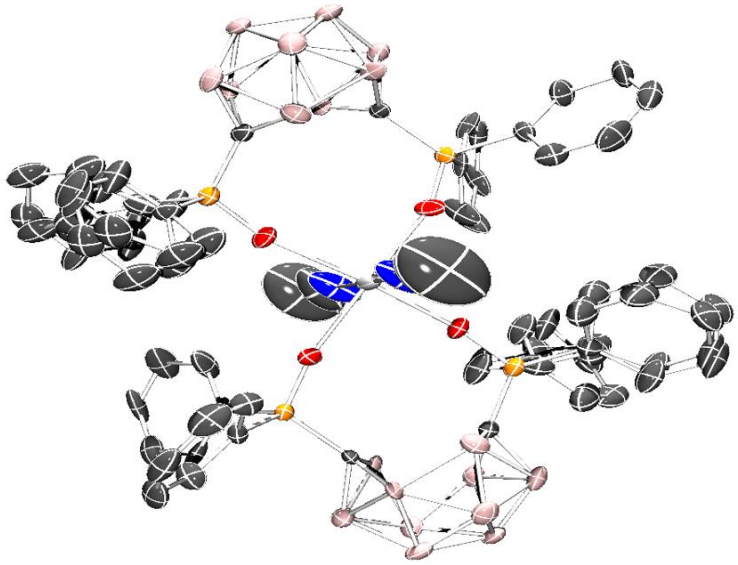

Figure 3.2. Solid-state molecular structure of $[K^+]_2[Dy(^{PO}Cb)_2](CNCH_3)_2$. H atoms, K+ counter cations, , and all co-crystallized solvent molecules are omitted for clarity. Selected bond lengths: Dy1-O1 2.274 Å Dy1-O2 2.304 Å, C-C 2.848 Å. C, black; N, blue; O, red; P, orange; Dy, gray

Erbium (Er) is forming a 6 coordinate cluster with 2 carboranes and 2 acetonitrile molecules.The average C-C bond length of carboranes in a cluster is 2.86 Å and the total cluster has charge of -1. One potassium is around to balance the charge.**(Figure 3.3)**

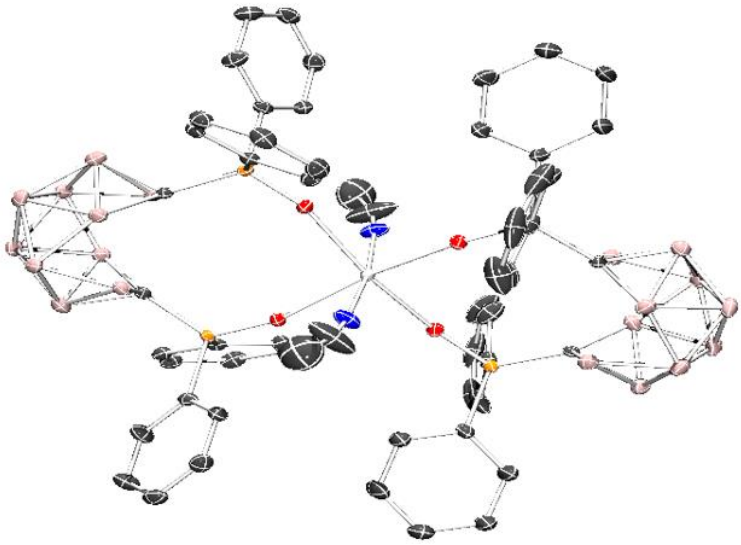

Figure 3.3 Solid-state molecular structure of $[K^+]_2[Er(POCb)_2](CNCH_3)_2$. H atoms, K+ counter cations, and all co-crystallized solvent molecules are omitted for clarity. Selected bond lengths: Er1-O1 2.163 Å Er1-O2 2.182 Å, C-C 2.848 C-C 2.872

Cerium (Ce) is forming a 6 coordinate cluster with 2 carboranes and 2 acetonitrile molecules.The average C-C bond length of carboranes in a cluster is 2.847 Å and the total cluster has charge of -1. One potassium is around to balance the charge.**(Figure 3.3)**

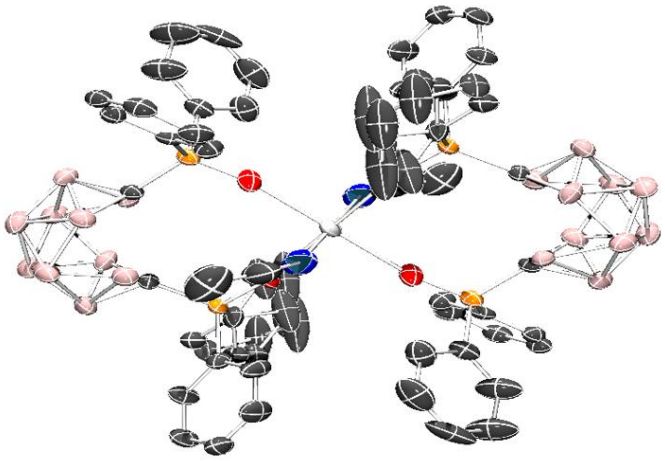

Figure3.4 Solid-state molecular structure of $[K^+]_2[Ce(POCb)_2](CNCH_3)_2$. H atoms, K+ counter cations, and all co-crystallized solvent molecules are omitted for clarity. Selected bond lengths: Ce1-O1 2.309 Å Dy1-O2 2.311 Å, C-C 2.855, 2.839

The rest of the lanthanide metal formed 3 adducts of carborane per metal. To our surprise, the reaction with Ho**(Figure 3.5)** and Tb**(Figure 3.6)** and Eu with *nido*-^{PO}Cb resulted in 3 adducts per metal after the addition of 2.1 eq. of *nido*-^{PO}Cb , **2**. Some clusters with 3 adducts of the carborane were not charge balanced. Pr, Sm, Nd showed a 3:1 adduct coordinated structure with charge balanced. We determined that it seemed like it is missing potassium to balance the charge from the XRD data. There showed some deficient amount of positive charge, meaning we need more potassium(+1) in the XRD data but couldn't find more of the potassium. To explain why the charge is not balanced, we suspected the Cb is not a -2 charge state but a -1 charge state. To check if our hypothesis is right, we checked the bond length between carbon and carbon in Cb. A less pronounced elongation of the C-C distance in the nido form could

indicate partial reduction of the closo-Cb. The studies showed that the *nido*- Cb C-C bond distance in mono-reduced ^{po}Cb is shorter than ***2*** (2.855 Å)[4] in some cases which the Cb cluster was not completely opened up. The solid-state structure of the adducts with Tb showed a distinct smaller distance C···C: 2.609Å, which may suggest one of the Cb clusters was mono-reduced with a -1 charge. However, the solid-state structure of Ho and Eu adduct showed almost no change in C-C bond distance so cannot back up the fact that it is having less charge on Cb like Tb.

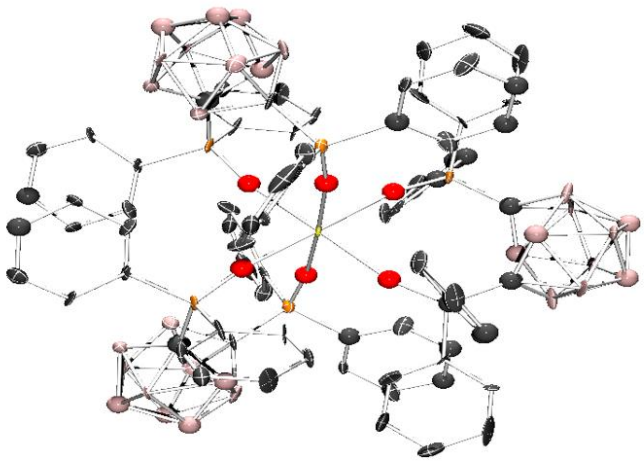

Figure3.5 Solid-state molecular structure of **[K]$_2$[Ho(^{PO}Cb)$_3$]**. H atoms, K + counter cations, phenyl C–H linkages, and all co-crystallized solvent(acetonitrile) molecules are omitted for clarity. Ho-O 2.244, Ho-O 2.272, C-C 2.885

Missing 1 K+

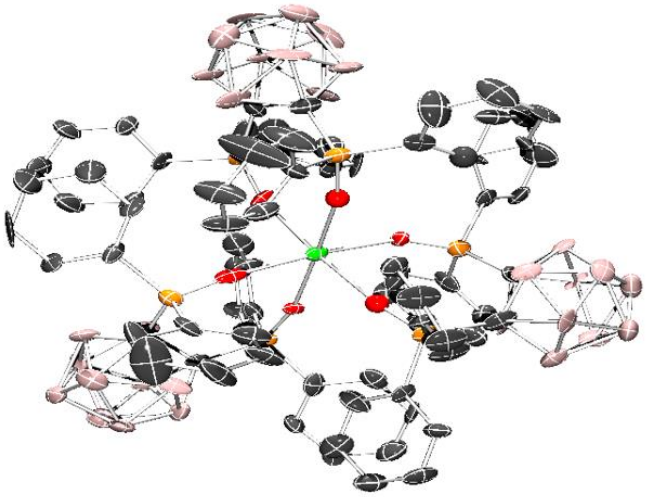

Figure3.6 Solid-state molecular structure of **$[K]_2[Tb(POCb)_3]$.** H atoms, K+ counter cations, phenyl C–H linkages, and all co-crystallized solvent molecules are omitted for clarity.

Selected bond lengths: Tb1-O1 2.241 Å Tb1-O2 2.285 Å, C-C 2.824, 2.609

Missing 1 K+

The divalent oxidation state has been reported for all the lanthanides (except radioactive Pm) and is relatively common for a few lanthanides ($Eu^{2+,}$ Sm^{2+}, and Yb^{2+}).[8] This was expected based on calculated generic Ln3+/Ln2+ reduction potentials **(Table 3.2).** Looking at the possibility that lanthanide can reduce each other, another suggestion for explaining charge imbalance can be brought up. Lanthanide metals might have reduced and oxidized each other making the lanthanide state not +3 but +2 or might have oxidized $[^{PO}Cb]^{-2}$. Since we were reacting 2.1 :1 ratio of the species, there we had some excess amount of lanthanide metal relative to *nido*-^{PO}Cb after forming the 3:1 cluster. We looked at the reduction potential of Tb, Dy, and Ho **(Table 3.3)**, to probe whether the excess metal was oxidizing *nido*-^{PO}Cb or

reducing the metal itself. Tb and Ho had no more negative reduction potential than other lanthanides that showed balanced charged cluster (Dy, Nd, Pr, etc.) but Eu had higher reduction potential than any other lanthanides. This information gives hint of why Eu showed the least charge balanced state among the lanthanides cluster (missing more than 2 potassiums) Also, Eu has the possibility of oxidizing *nido*-^{PO}Cb resulting Eu +3 to +2. However, for Ho and Tb, it is inconclusive to say that it shows the charge is not balanced due to the high reduction potential.

New experiments were conducted with 3 eq. of **2** coordinating with 1 eq. of different Lanthanide metals like Tb, Dy, and Ho. **(Table 3.3).** Tb and Ho adduct still showed the deficient amount of positive charge revealed by solid-state structure obtained by single crystal XRD studies. The amount of positive charge missing was not the same as in the previous experiment where you reacted 2.1eq of *nido*-^{PO}Cb with 1 eq. of lanthanide metal. The Dy adduct that formed a cluster 2:1with 2.1 eq :1 eq experiment, showed a 3:1 cluster with the correct charge balanced.

Element	Element number	10^3 M	Reduction	E 1/2 (V)
Pr	59	0.976	$3e^-$	-1.47
Nd	60	0.989	$3e^-$	-1.49
Sm	62	0.994	III -> II	-1.13
Eu	63	1.101	III -> II	-0.03
Gd	64	0.496	$3e^-$	-1.49

Tb	65	1.038	$3e^-$	-1.38
Dy	66	1.144	$3e^-$	-1.44
Ho	67	0.983	$3e^-$	-1.44
Er	68	1.027	$3e^-$	-1.43
Tm	69	0.994	$3e^-$	-1.44
Yb	70	0.997	III -> II	-0.71

Table 3.2 Reduction potential of Lanthanides (vs. SCE) [6]

Atom number	**65**	**66**	**67**
Lanthanide types	**Tb**	**Dy**	**Ho**
Number of Carborane per lanthanide metal	**3**	**3**	**3**
Charge balance	**Missing 1.5K more**	**Charge balanced**	**Missing >2K**
C-C bond length after coordination	**2.865 2.865 2.865**	**2.814 2.824 2.814**	**2.772 2.816 2.847**

Table 3.3 *nido*-^{PO}Cb coordinating(3 eq) with different Lanthanide metals (1 eq.)

3.3 Summary

In this chapter, we were able to discover that the increased bite angle of *nido*-^{PO}Cb was enough to coordinate with sized lanthanides compared to uranyl. We reacted 2.1 eq of *nido*-^{PO}Cb with 1 eq lanthanide metal in the form of $Ln(NO_3)_3THF_3$ and were able to observe 2 types of clusters, 2:1 and 3:1 (carborane: lanthanide metal). Anecdotally, Dy formed 2:1 cluster, and Tb exhibited 3:1 cluster. To our surprise, 2:1 cluster showed all charge balanced coordinated clusters whereas most of the 3:1 clusters showed non-charge balanced clusters with missing potassiums. This tendency of none charge balanced cluster emerged again even though the change of equivalent of *nido*-^{PO}Cb to 3 equivalent. In this chapter, we were able to extend the metal species category from uranyl to lanthanide metal. However, further study is needed to understand the characteristic of each lanthanide which shows different coordinating clusters depending on what kind of lanthanide metal we use.

3.4 Experimental

General Considerations. All manipulations were carried out under an atmosphere of dry, oxygen-free N_2 within an MBraun glovebox (MBRAUN UNIlab Pro SP Eco equipped with a −35 °C freezer), or by standard Schlenk techniques. Pentane, hexanes, benzene, Et_2O, DCM, DCE and THF (inhibitor-free) were dried and degassed on an MBraun Solvent Purification System and stored over activated 4 Å molecular sieves. Celite and 4 Å molecular sieves were dried at 250 °C under dynamic vacuum (<0.1 Torr) for 24 h prior to use. All reagents were obtained from Sigma-Aldrich, Fisher Scientific, or VWR.

Spectroscopic Measurements. NMR spectra were obtained on an Agilent Technologies 400 MHz DD2, Varian Unity Inova 500 MHz, Bruker Avance NEO 500 MHz, or a Varian 600

MHz spectrometer, and referenced to residual solvent. Chemical shifts (δ) are recorded in ppm and the coupling constants are in Hz. J. Young airtight adaptors were used for air- and water-sensitive compounds. All measurements were carried out on recrystallized product. All stock solutions and dilutions were prepared by mass or volume.

X-ray Crystallography. Data were collected on a Bruker KAPPA APEX II diffractometer equipped with an APEX II CCD detector using a TRIUMPH monochromator with a Mo Kα X-ray source (α = 0.71073 Å). The crystals were mounted on a cryoloop under Paratone-N oil, and all data were collected at 110 K using an Oxford nitrogen gas cryostream system. A hemisphere of data was collected using ω scans with 0.5° frame widths. Data collection and cell parameter determination were conducted using the SMART program. Integration of the data frames and final cell parameter refinement were performed using SAINT software. Absorption correction of the data was carried out using SADABS. Structure determination was done using direct or Patterson methods and different Fourier techniques. All hydrogen atom positions were idealized and rode on the atom of attachment. Structure solution, refinement, graphics, and creation of publication materials were performed using SHELXTL or OLEX[2].

Synthesis of $[K]_2[(nido\text{-}1,2\text{-}(Ph_2PO)_2\text{-}1,2\text{-}C_2B_{10}H_{10})]$

Step 1. In the glovebox, a 250-ml round-bottom flask equipped with a magnetic stir bar was charged with 1 (272.2 mg, 0.5 mmol) and 20 ml of THF, and cooled to −78 °C. In a separate vial, KC8 (182.4 mg, 1.35 mmol, 2.7 equiv.) was suspended in 20 ml of THF and added slowly dropwise to the stirring solution of **1**. Upon addition, the KC8 suspension began to turn grey

and was stirred for 30 min at room temperature. Stirring was discontinued and the mixture was filtered over a pad of celite on a fine glass frit. The graphite pad was washed additionally with MeCN (3 × 5 ml). The filtrate was collected and the volatiles was removed in vacuo, yielding a pale-yellow oil. The oil was redissolved in THF (5 ml) and layered with 5 ml of pentane and recrystallized at −38 °C, yielding a white solid. (Yield 15.8%) X-ray crystallography were obtained by vapor diffusion of Et2O in a saturated THF solution of **2** at −38 °C.

Synthesis of [CoCp$^*_2$]$_2$ [(*nido*-1,2-(Ph$_2$PO)$_2$-1,2-C$_2$B$_{10}$H$_{10}$)]

The product is known in the literature.[1]A 20-ml vial equipped with a magnetic stir bar was charged with 1 (54.4 mg, 0.1 mmol) and 6 ml of benzene. In a separate vial, CoCp*2 (69.1 mg, 0.2 mmol, 2.0 equiv.) was dissolved in 4 ml of benzene and added dropwise to the stirring solution of 1. Upon addition, a yellow solid immediately precipitated from the reaction mixture, and the mixture was stirred for an additional 4 h at room temperature. Stirring was discontinued and the solid was allowed to settle to the bottom of the vial. The supernatant was decanted and filtered on a plug of celite. The solids were washed with benzene (3 × 6 ml) and each washing was filtered over the same celite plug. The remaining solids were then dis-solved in a minimal amount of MeCN (2 ml) and filtered on the same celite plug into a new vial. The MeCN filtrate was collected and the volatiles was removed in vacuo, yielding a shiny golden-yellow solid (114.3 mg, 0.95 mmol, 95% yield). Single crystals suitable for X-ray crystallography were obtained by vapor diffusion of Et2O in a saturated MeCN solution of 2a at −38 °C. (Yield >99%)

Synthesis of [CoCp* $_2$]$_3$[Pr(POCb)$_3$]

A 20 mL vial equipped with a magnetic stir bar was charged with $[CoCp^*_2]_2[^{PO}Cb]$ and 2 mL of MeCN. In a separate vial, $[Pr(NO_3)_3(THF)_3]$ was dissolved in 2 mL of MeCN and then added dropwise to the stirring solution of $[CoCp^*_2]_2[^{PO}Cb]$, where the solution was bright yellow, with no change in color after the addition of lanthanide metal. The solution remained homogenous and the reaction was stirred at room temperature for 4 h.

The volatiles was removed in vacuo, yielding a yellow powder. The powder was washed with THF (8 mL) and the mixture was transferred onto a bed of Celite on a glass frit. The yellow solid was washed with additional THF (3 x 2 mL). The filter was then dissolved in MeCN into a new vial. The MeCN filtrate was collected and the volatiles was removed in vacuo, yielding a yellow powder. Residual $[CoCp^*_2][NO_3]$ was removed from this crude yellow solid by repeated selective recrystallizations (2-3 times) by vapor diffusion of Et2O into a concentrated pyridine solution of the crude solid at -38 °C. The supernatant was then transferred and the volatiles was removed yielding a yellow solid. Single crystals suitable for XRD studies were grown by vapor diffusion of Et_2O into a saturated MeCN solution of $[CoCp^*_2]_3[Pr(^{PO}Cb)_3]$ at room temperature. (Yield 39.5%)**^{1}H NMR** (400 MHz, $CDCl_3$): δ 10.78 (broad, 10H), 7.95 (broad, 10H), 7.52 (broad, 5H), 4.97 (broad, 5H), 3.47 (broad, 10H), 1.70 (90H , Cp^*), 0.84(broad, 20H), -0.47 (broad, 10H) Carborane **^{11}B {^{1}H} NMR** (128 MHz, $CDCl_3$): was too broad to be observed. **^{31}P {^{1}H} NMR** (162 MHz, $CDCl_3$): δ 121.63

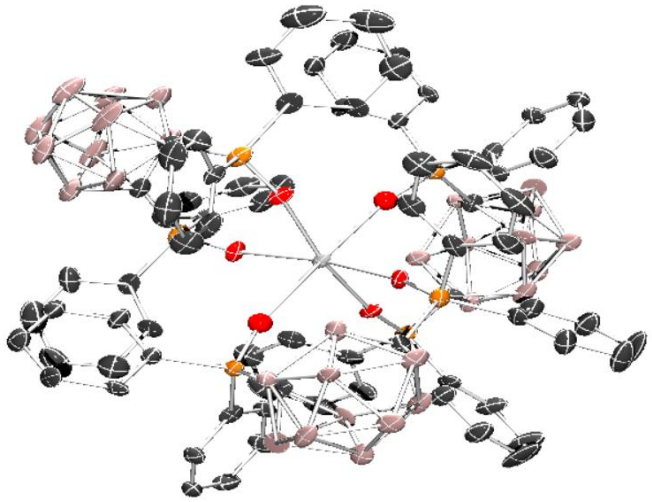

Figure 3.7 Solid-state molecular structure of **[CoCp* $_2$]+[Pr(POCb)$_3$]**. H atoms, [CoCp* 2] + counter cations, phenyl C–H linkages, and all co-crystallized solvent(acetonitrile) molecules are omitted for clarity.Pr-O 2.364, Pr-O 2.341, C-C 2.811, 2.725

Synthesis of Lanthanide cluster with [K]$_2$[^{PO}Cb]THF$_4$

A 20 mL vial equipped with a magnetic stir bar was charged with [K]$_2$[^{PO}Cb]THF$_3$and 2 mL of MeCN. In a separate vial, [Ln(NO$_3$)$_3$(THF)$_3$] was dissolved in 2 mL of MeCN and then added dropwise to the stirring solution of [K]$_2$[^{PO}Cb]THF$_3$, where the solution was transparent, the solution becomes cloudy after addition of lanthanide metal. The solution remained homogenous and the reaction was stirred at room temperature overnight.

The mixture was transferred onto a bed of Celite on a glass frit getting rid of the solid KNO$_3$. The filter was then dissolved in MeCN into a new vial. The MeCN filtrate was collected and the volatiles was removed in vacuo, yielding a yellow powder. The supernatant was then

transferred and the volatiles was removed yielding a yellow solid. Single crystals suitable for XRD studies were grown by vapor diffusion of Et_2O/pentane/hexane into a saturated MeCN solution of $[K]_x[Ln(^{PO}Cb)_3]$ at room temperature. Yield was calculated in **Table. 3.4**

Compound	Yield
$[K]_3[Tb(^{PO}Cb)_3]$	25.4%
$[K][Er(^{PO}Cb)_2]$	36.3%
$[K]_3[Ho(^{PO}Cb)_3]$	16.2 %
$[K][Dy(^{PO}Cb)_2]$	31.5%
$[K][Ce(^{PO}Cb)_2]$	19.6%
$[K]_3[Eu(^{PO}Cb)_3]$	Too trivial amount to calculate yield.

Table 3.4 Yield of *nido*-^{PO}Cb coordinating (2.1eq) with different Lanthanide metals (1eq.)

Preparation of Ln $(NO_3)THF_3$

In a dried schlenk flask, a solution of $Ln(NO_3)_3H2O_6$ (1eq) in trimethyl orthoformate (12eq) was stirred under nitrogen for 14h, All volatile is distilled under reduced pressure, and then dries the residue for 14h at 0.1Torr. Brought into the glove box and then add cooled THF (7eq) and stir for 2h. Remove solvent in vacuo and add THF (7eq), stir for 2h, and remove the solvent in vacuo again. Recrystallized with THF at room temperature and lowered the temperature to -38ºC.

Synthesis of $[K]_x[Ho(^{PO}Cb)_3]$

A 20 mL vial equipped with a magnetic stir bar was charged with $[K]_2[^{PO}Cb]THF_3$and 2 mL of MeCN. In a separate vial, $[Ho(NO_3)_3(THF)_3]$ was dissolved in 2 mL of MeCN and then added dropwise to the stirring solution of $[K]_2[^{PO}Cb]THF_3$, where the solution was transparent, the solution becomes cloudy after addition of lanthanide metal. The solution remained homogenous and the reaction was stirred at room temperature overnight.

The mixture was transferred onto a bed of Celite on a glass frit getting rid of the solid KNO_3. The filter was then dissolved in MeCN into a new vial. The MeCN filtrate was collected and the volatiles was removed in vacuo, yielding a yellow powder. The supernatant was then transferred and the volatiles was removed yielding a yellow solid. Single crystals suitable for XRD studies were grown by vapor diffusion of Et_2O/pentane/hexane into a saturated MeCN solution of $[K]_x[Ho(^{PO}Cb)_3]$ at room temperature.(16.2 %) **^{1}H NMR** (400 MHz, $CDCl_3$): δ 4.20 (m, 10H), 1.95 (broad, 20H), 1.68 (broad, 5H), 1.38 (m, 30H), 0.93 (m, 20H), -0.98 (broad, 5H)**^{31}P {^{1}H} NMR** (162 MHz, $CDCl_3$): δ -120.65 (broad)

3.5 Reference

1. Nourry, C.; Soucek, P.; Glatz, J.; Kato, T. Advanced Fuel Cycle Options *Asian Nuclear Prospects 2010, No 10.* **2011**

2. Cotton, S. A. Scandium, Yttrium & the Lanthanides: Inorganic & Coordination Chemistry; Uppingham School **2011**.

3. E. Clementi, D.L.Raimondi,, W.P. Reinhardt. Atomic Screening Constants from SCF Functions. II. Atoms with 37 to 86 Electron. *Journal of Chemical Physics.* **1967** *47*: 1300.

4. Keener, M.; Hunt, C.; Carroll, T. G.; Kampel, V.; Dobrovetsky, R.; Hayton, T. W.; Ménard, G. Redox-Switchable Carboranes for Uranium Capture and Release. *Nature* **2020**, *577 (7792)*, 652–655..

5. Union, I.; Pure, O. F.; Chemistry, A. Solubility Data Series; 1991; Vol. 47.Union, I., Pure, O. F. & Chemistry, A. *Solubility Data Series. Alkali Metal and Ammonium Chlorides in Water and Heavy Water (Binary Systems)* **1991***vol. 47*

6. Couffin, F. Redox Potential of Lanthanides and Actinides Elements in Organic Solvents. **1980**, 84 pp.

7. Keener, M.; Mattejat, M.; Zheng, S. L.; Wu, G.; Hayton, T. W.; Ménard, G. Selective Electrochemical Capture and Release of Uranyl from Aqueous Alkali, Lanthanide, and Actinide Mixtures Using Redox-Switchable Carboranes. *Chem. Sci.* **2022,** 13 (12), 3369–3374.

8. Valentin Guidal, Biplab Biswas, and P Jacques, 'EDGE ARTICLE Cl', *Sci, Chem*, **2012**, 2433–48

9.Heiserman, D.L. Exploring Chemical Elements and Their Compounds. Blue Ridge Summit, PA: TAB Books, **1992.**

10.Lide, D.R., ed. CRC Handbook of Chemistry and Physics. 74th ed., Boca Raton, FL: CRC Press, **1991.**

11. Niemeyer, M. 1,2-Dimethoxyethan- Und Tetrahydrofuran-Komplexe Der *Anorg. und Allg. Chemie* **2006**, *632* (8–9), 1449–1456.

13. Nilsson, M.; Ekberg, C.; Foreman, M.; Hudson, M.; Liljenzin, J. O.; Modolo, G.; Skarnemark, G. Separation of Actinides(III) from Lanthanides(III) in Simulated Nuclear Waste Streams Using 6,6′-Bis-(5,6-Dipentyl-[1,2,4] Triazin-3-Yl)-[2,2′]Bipyridinyl (C5-BTBP) in Cyclohexanone. *Solvent Extr. Ion Exch.* **2006**, *24* (6), 823–843.